



# Geochemical and isotopic characterization of groundwater and identification of hydrogeochemical processes in the Berrechid aquifer of central Morocco

Tibari El Ghali<sup>1,2</sup> · Hamid Marah<sup>1</sup> · Mohamed Qurtobi<sup>1</sup> · Fatima Raibi<sup>1</sup> · Miriam Bellarbi<sup>1</sup> · Nourddine Amenzou<sup>1</sup> · Bouâbid El Mansouri<sup>2</sup>

Accepted: 24 February 2020 / Published online: 9 March 2020  
© Springer-Verlag GmbH Germany, part of Springer Nature 2020

## Abstract

The hydrogeochemical characteristics and processes affecting the groundwater chemistry of the Berrechid Basin, central Morocco, were determined using chemical and isotopic data from 71 groundwater and six surface water samples. Chemical data shows a wide variation in mineralization, notably exceeding the permissible level of potability. Unlike the northern area, which seems to be separate from the main system, the salinity profile demonstrates a rising trend from the intake area in the south to the downstream area in the east and west, where the groundwater becomes more saline. Three basic hydrogeochemical facies are distinguished: Na–Cl, Na–Mg–Ca–Cl, and Ca–Mg–HCO<sub>3</sub>–Cl. A trend was also noticed for the last two types toward Na–Cl. Chemical composition of the groundwater is mainly determined by the influence of evaporation, cation exchange, rock weathering, salt dissolution, and anthropogenic activities. The dolomitization process has also been put forward as an explanation for groundwater saturation with respect to the carbonate minerals, particularly in the eastern and western parts. The groundwater is enriched with <sup>2</sup>H and <sup>18</sup>O, which independently, as well as with Cl<sup>-</sup> and NO<sub>3</sub><sup>-</sup>, strengthens the findings from the chemical data by affirming the dominant effects of evaporation, the dissolution of minerals, and anthropogenic activities in assessing the geochemical evolution of the groundwater. Furthermore, this allows a twofold identification of recharge sources in the Berrechid aquifer: a lateral flow from the Phosphate Plateau, mainly along the southern part of the basin, and a vertical downward movement of evaporated water from rainfall, rivers, and the return of irrigation flow.

**Keywords** Geochemistry · Isotopes · Groundwater · Salinity · Evaporation · Berrechid basin

## Introduction

The development of groundwater resources for water supply is a prevalent practice in Morocco. The Berrechid Basin with its fertile soil is particularly productive, and its considerable groundwater resources contribute greatly to the region's socio-economic development (Elfarrak et al. 2014).

Nonetheless, the groundwater in the Berrechid Basin faces a serious threat from overexploitation for irrigation, while domestic/industrial uses have substantially increased the abstraction and pollution of groundwater and induced notable changes in the hydrologic system. Indeed, agricultural development has led to a discernible rise in the drawdown of regional groundwater level and significant environmental issue of groundwater pollution (El Bouqdaoui et al. 2008; El Assaoui et al. 2015). The population of the Berrechid basin was only around 712 in 1926, but it had grown to 484,518 habitants in 2014 (HCP 2015). According to a survey released by the Basin Agency of Bouregreg and Chaouia (ABHBC 2005), the total irrigated area and the abstraction rate have increased from 7147 to 13,300 ha and 46 Mm<sup>3</sup>/y to 58 Mm<sup>3</sup>/y, respectively, between 1986 and 2007, leading to a deficit of 20 Mm<sup>3</sup>. What is more, the groundwater vulnerability assessment of the area reports a high level of susceptibility to contamination (Ait Sliman et al. 2009; Elfarrak

**Electronic supplementary material** The online version of this article (<https://doi.org/10.1007/s13146-020-00571-y>) contains supplementary material, which is available to authorized users.

✉ Tibari El Ghali  
elghali.tibari@gmail.com

<sup>1</sup> National Center for Energy Sciences and Nuclear Techniques, BP. 1382, R.P. 10001 Rabat, Morocco

<sup>2</sup> Laboratory of Geosciences/Natural Resources, Ibn Tofail University, BP. 133, Kenitra, Morocco

et al. 2014; Aboulouafa et al. 2016), as well as critical levels of groundwater pollution due to anthropogenic activities, wastewater leaching, and the use of large amounts of fertilizers in agriculture (Kholtei et al. 2003; El Bouqdaoui et al. 2009).

Although considerable studies focus on the behavior of the dynamic system in the Berrechid Basin (El Mansouri et al. 1992; El Mansouri 1993; ABHBC 2005; Droubi et al. 2008; El Bouqdaoui et al. 2008; Smaoui et al. 2012; El Assaoui et al. 2015), the field remains in its infancy, so the factors controlling the chemical composition of the groundwater are still little known. Few studies have dealt with weathering reactions and solute acquisition by meteoric water (Hazan and Moullard 1962) for example. There are also limited recent hydrogeological studies conducted in the basin, comprising just the reports published by the Hydraulic Basin Agency of Bouregreg and Chaouia (ABHBC) based on the hydrological monitoring of wells and springs in the area. These studies remain insufficient to characterize the groundwater recharge and chemical evolution or to describe the geochemical processes taking place in the system in response to local reactions conditions.

The sustainable management of groundwater resources requires a large degree of available knowledge and information about understanding the aquifer hydraulic properties and the chemical composition variation. The behavior of groundwater chemistry is influenced by several factors, such as climate, the quality of recharge water, geology, residence time, the manner of groundwater's flow through the rock types (dissolution, precipitation, and cation exchange) from recharge to discharge areas, and inputs from other anthropogenic activities (Freeze and Cherry 1979; Hem 1985; Appelo and Postma 1993).

Over recent decades, geochemical methods have contributed greatly to understanding how structural, geological, mineralogical, and hydrological features control the flow and chemistry of these systems (Lakshmanan et al. 2003; Rajmohan and Elango 2004, 2006; Srinivasamoorthy et al. 2008; Hamed and Dhahri 2013; Zaidi et al. 2015; Bozdağ 2016). Likewise, isotopic techniques are broadly used in Morocco, and they act as effective tools in hydrogeology for identifying groundwater recharge origins and evolutionary trends (IAEA 2010; Qurtobi et al. 2010). Indeed, several investigations have used geochemical and isotopic techniques to evaluate the sources of recharge and the chemical evolution (Dindane et al. 2003; Bouchaou et al. 2008; 2009; Al-Charideh and Abou-Zakhem 2010; Srinivasamoorthy et al. 2011; Abderamane et al. 2013; Warner et al. 2013; Liu et al. 2014; Ait Brahim et al. 2015; Boukhari et al. 2015). Thus, geochemical and isotopic methods are clearly important tools for developing sustainable, integrated water-management policies for protecting water resources. Hence, the primary purpose of this study is to employ chemical

and isotopic analyses to contribute to a better understanding of the hydrochemical characteristics of groundwater but also to identify the hydrological and geochemical processes responsible for the chemistry and the recharge origins of the Berrechid Basin in central Morocco.

## Study area

The study area, the Berrechid basin, covers an area of approximately 1500 km<sup>2</sup> in the southern part of the province of Casablanca in the central portion of Morocco (Fig. 1a). The region's climate is semi-arid and influenced by the North Atlantic air masses that circulate from the west over northern Africa (the air humidity gradient is determined by the distance from the coast, with fog commonly forming in winter), as well as the Mediterranean air masses that circulate from the north (El Ghali et al. 2018b). Thus, this configuration of geographic flow opens the way to the overflow of cold air masses in winter and the sea breeze to refreshes the atmosphere in summer. The long-term mean annual rainfall ranges between 280 and 310 mm, with 93% of precipitation occurring during the rainy season, which lasts for about seven months between October and April. The dry season typically comprises a dry spring and the summer months, lasting for about four months between May and September. The mean annual temperature is about 19.04 °C, with temperatures reaching about 26.43 °C in summer (in August) and dropping to a low of 6.38 °C in January. The potential evapotranspiration is about 946.59 mm/year (ABHBC 2005). The main socio-economic activities in the Berrechid basin are livestock and cereals.

Topographically, the basin is a flat area and characterized by elevations and gradients ranging from 140 m and 0.2%, respectively, in the north to 350 m and 0.8% in the southern portion (El Assaoui et al. 2015). It is bounded on the south by the Phosphate Plateau, by the El Mellah Valley on the northeast, by the Chaouia plain to the north, and by primary outcrops to the west and northwest (Fig. 1a) (ABHBC 2005).

The Berrechid basin's geology has been broadly studied over time (Ruhad 1975; El Mansouri 1993; Lyazidi et al. 2003; El Gasmî et al. 2014) and the findings of the available geological studies have been examined. The Berrechid Plain forms part of the marine area of the western Moroccan Meseta. Its complex tectonic history has been marked by several periods of transgression and regression of the sea. During the Pliocene Epoch, carbonate and evaporitic sediments were deposited (Ruhad 1975; Lyazidi et al. 2003). Under semi-arid climatic conditions, combined with the very old subsidence and sedimentation ranging in age from primary to recent sediments, various geological formations were deposited in the form of a wide bowl (Hazan and Moullard 1962). From bottom to top of the



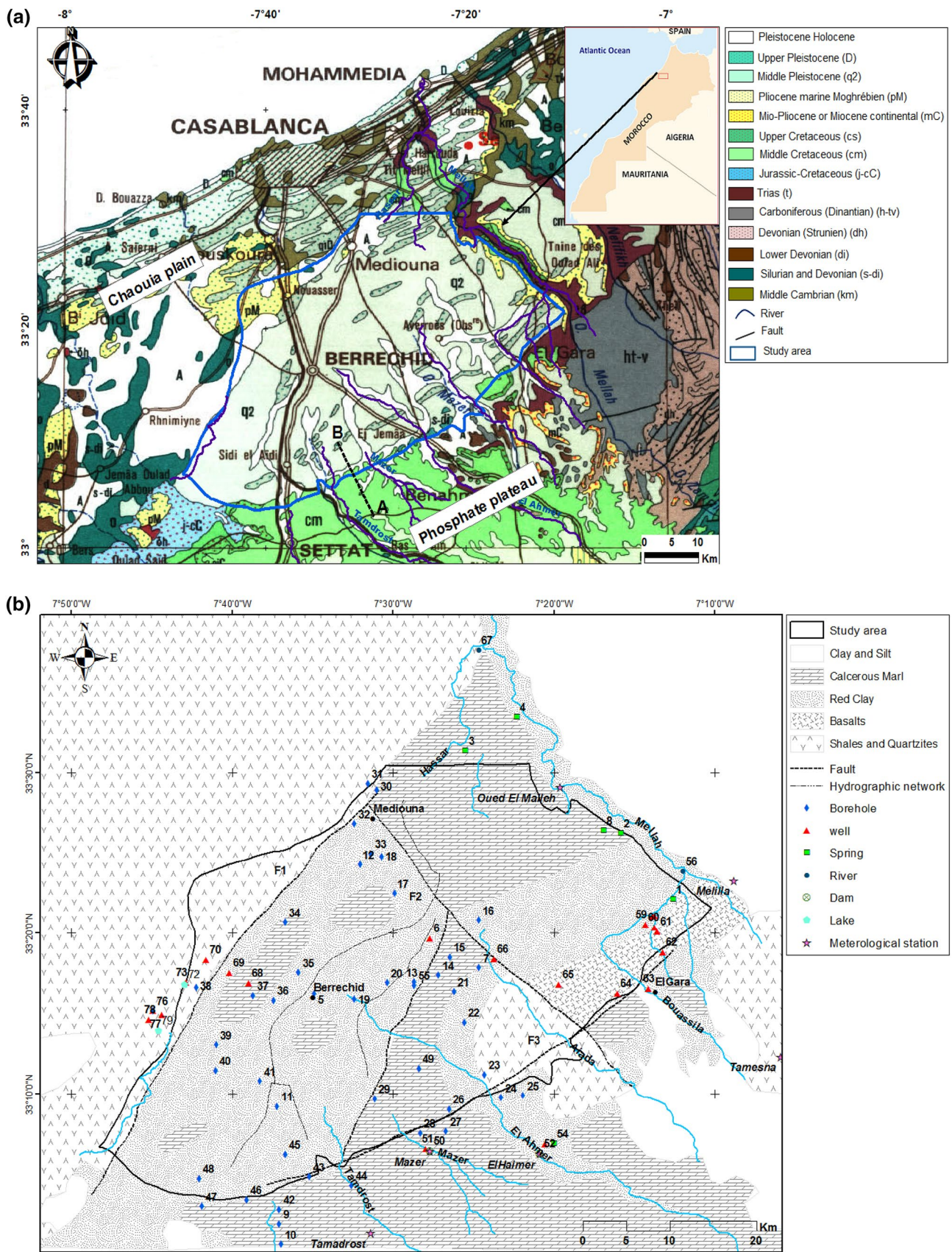


**Fig. 1** a Location and geological time of the Berrechid basin (Saadi et al. 1985), b geology of the basement and sample locations in the study area (ABHC 2005), c geoelectric section along AB in the Phosphate plateau-Berrechid basin (El Gasmii et al. 2014)

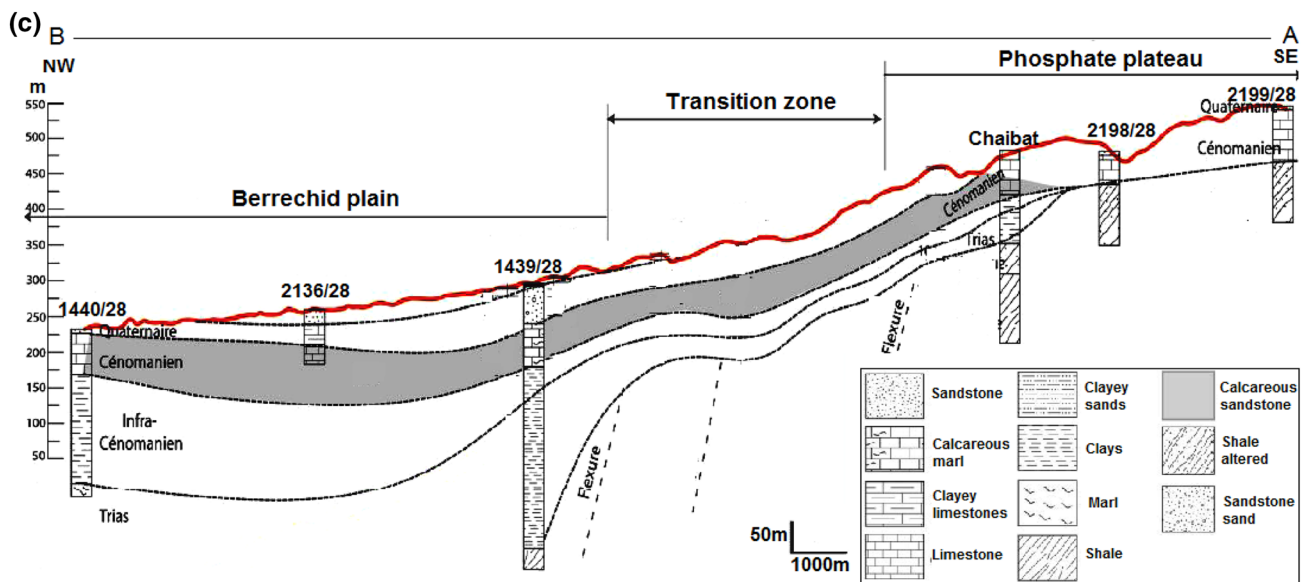


Fig. 1 (continued)

stratigraphic scale, the litho-stratigraphic sequence of the formations encountered is presented as follows (Fig. 1b, 1c): *Primary*: The bedrock consists of schist intercalated by layers of sandstone and quartzite. The main outcrops are Silurian and Devonian along the southeast and green Acadian alongside the northwest, along with 150-m-thick Mediouna and Bouskoura close to El Hank (El Mansouri et al. 1992; Smaoui et al. 2012). *Triassic*: The deposits here are characterized by siliciclastic and saliferous red clays intercalated by minor basalts and evaporates (e.g., rock salt, potash, gypsum). These are distributed in the northeast portion west of the city of El Gara, and they gently dip under the Cenomanian deposits toward the southwest (El Mansouri 1993; Lyazidi et al. 2003; Bensalah et al. 2011). *Infra-Cenomanian*: These consist of detrital red clays that are rich in gypsum, sometimes with some conglomerate levels followed by layers of white-to-yellow marls and limestone, with a total thickness of 40 m (Ruhad 1975). *Cenomanian*: These sediments comprise yellow marls and dolomitic limestone with greenish marl intercalations for a thickness of 120 m. *Pliocene*: These form the main regional aquifer of the Berrechid Basin and comprise sands, sandstones, sandy limestone, and minor conglomerates at the base for a total thickness ranging from 5 to 40 m (Droubi et al. 2008). *Quaternary*: The Quaternary deposits are the prevailing facies and fundamentally comprise silt and conglomerate series followed by red silty clays and then pebbles and gravel at thicknesses of 0–50 m. At low elevations in the upstream part of the catchment basin, widespread alluviums (silt and gravels) have been shaped as a result of erosion and then moved

by water streams (seasonal wadis), such as flash floods, or by the wind during dry periods. These layers provide confined conditions for the Berrechid aquifer, which is only unconfined in the center.

Tectonic movements in the basin have resulted in three normal faults (Fig. 1b): fault F1 in a NNE-SSW direction, which passes by Mediouna and creates a tectonic boundary between the primary bedrock and post-Triassic formations; fault F2, which orients in a NW-SE direction and joins fault F1 in Mediouna; and fault F3 that moves in a NE-SW direction and passes by El Gara and defines the SE limit of the Berrechid Basin (ABHBC 2005). Depending on the aquifer thickness, the storage coefficient and transmissivity vary from 0.5 to 3.5%, respectively, and from  $2.8 \times 10^{-4}$  at the borders to  $2.8 \times 10^{-1} \text{ m}^2/\text{s}$  at the center. The direction of flow goes toward the north and the northeast of the plain, thus reflecting the regional topographic gradient (Droubi et al. 2008). According to the water recharging the Berrechid aquifer derives from (i) lateral inflow from the Phosphate Plateau aquifer (ii) infiltration from the surface, such as through rainfall and seasonal rivers (El Himmer, Mazer, Tamdrost, Boumoussa, Bouassila), and (iii) the return flow of water from irrigation and wastewater. The flow rate of the seasonal rivers is controlled by dams (El Himmer, Mazer, Tamdrost) that were constructed to prevent periodic floods and provide artificial recharge. The discharge of water from the Berrechid aquifer takes place by pumping water for irrigation and drinking purposes, as well as a lateral flow towards Chaouia Plain and the valley of the El Mellah in the form of a few local springs (El Bouqdaoui et al. 2008).



## Materials and methods

Over the period of this study, three sampling campaigns were conducted in April and July 2013 and March 2015. This resulted in the collection of a total of 71 groundwater samples from 45 boreholes, 20 wells, and 6 springs. What is more, because of the lack of rain measurements for the studied area, 41 precipitation samples were collected from the six closest stations located near the tributaries in the Berrechid Basin (Tamdrost, Mazer, El Haimer, El Maleh, El Gara, Tamasna). In addition, to evaluate the recharge-discharge relationship between the surface water and groundwater in the study basin, six surface-water samples were collected during the final sampling campaign at two different sites along the El Maleh River, two lakes, and two dams.

The sampling locations were selected based on spatial coverage within the aquifer. Most sampled points were used for private domestic supply, but others were agricultural and industrial water supplies or permanent monitoring wells. Depths ranged between 15 and 140 m. Shallow wells were usually finished near the top of the aquifer and generally located in the east and northwest of the plain, while deeper boreholes were mainly located in the parts between the south and north of the study area. Prior to sampling, all wells and boreholes were purged to remove stagnant water and ensure representative water samples. Physical parameters such as pH, temperature (T), and electrical conductivity (EC) were measured immediately in the field using portable field kits (Multi 440 Conductivity-pH meter). The total alkalinity (as  $\text{HCO}_3^-$ ) was determined through titration with 0.1 M HCl against phenolphthalein and helianthin indicators. Following this, polyethylene containers were perfectly rinsed using distilled water and filled with sample water. The collected samples were filtered using 0.45 mm Millipore filter paper and acidified with nitric acid for analysis. The samples were then placed in a refrigerator at 4 °C upon collection. Immediately following the collection of water samples, the analysis was performed at the Hydro Geochemistry Lab of the Department of Water and Climate Unit, National Center for Energy Sciences and Nuclear Techniques (CNESTEN), Rabat, Morocco.

The major ions ( $\text{Na}^+$ ,  $\text{K}^+$ ,  $\text{Ca}^{2+}$ ,  $\text{Mg}^{2+}$ ,  $\text{HCO}_3^-$ ,  $\text{Cl}^-$ ,  $\text{SO}_4^{2-}$ ,  $\text{NO}_3^-$ ) were analyzed through ion chromatography (Thermo scientific, Dionex ICS 5000<sup>+</sup> DC) with a limit detection of 0.1  $\mu\text{mol/l}$ . The quality of the water analyses was computed by taking the equivalent difference between the sums of cations and anions and dividing it by the sum of the cations and anions. Ion balance error for all samples was found to be within  $\pm 5\%$ . Total dissolved solids (TDS) was calculated by summing all the

concentrations of constituents, while the total hardness (TH) was determined using the following expression:  $\text{TH (as mg CaCO}_3) = (\text{Ca}^{2+} + \text{Mg}^{2+}) \text{ meq/l} \times 50$  (Hem 1985; Sawyer et al. 2003). The pressure of carbon dioxide ( $\text{pCO}_2$ ), saturation indexes (SI), and chemical facies of groundwater were determined by means of the Piper (1953) and PHREEQC (Parkhurst and Appelo 1999) computer programs. The default PhreeQC thermodynamic database was used to calculate all mineral saturation indexes.

For stable isotopes of oxygen and hydrogen, the measurement was carried out by employing the standard  $\text{H}_2$  and  $\text{CO}_2$  equilibration (Epstein and Mayeda 1953) followed by analysis on a DELTA PLUS mass spectrometer. The results for hydrogen and oxygen were reported in parts per mill (‰) in “ $\delta$ ” notation relative to Vienna-Standard Mean Oceanic Water (V-SMOW) with an analytical accuracy of  $\pm 0.1\text{‰}$  for  $\delta^{18}\text{O}$  and  $\pm 1\text{‰}$  for  $\delta^2\text{H}$ .

The spatial distribution maps were generated using the ordinary kriging method, which is one of the best spatial interpolation methods in the geostatistical gridding extension of the Golden Surfer software. Graphics were also created using the Microcal Origin 6 software. The groundwater quality was assessed by comparing it to the World Health Organization’s criteria for drinking water.

## Results and discussion

### Geochemical study

#### Groundwater chemistry

The statistical parameters—such as minimum, maximum, mean, and standard deviation—for different physical and chemical data for the groundwater were calculated. These are summarized with surface water characteristics and the maximum permissible limit in Table 1.

The pH of the groundwater ranges between 6.83 and 8.31 with an average of 7.32, indicating an alkaline trend for the groundwater. The acidic values were found in water from the southern and central parts of the study area, and these probably resulted from carbonates weathering or fertilizer use. While the higher pH values were found in water from the eastern and the western parts of the study area. Groundwater temperatures show relative heterogeneity, ranging between 17 and 25 °C. This reflects the possible influence of multiple factors, such as the depth of the groundwater, the residence time, and the groundwater’s flow time from the recharge to the discharge area. The concentration of major components within the study area demonstrates important variations, and each differs significantly in salinity and ionic composition, as reflected in the higher standard deviations for EC ( $\pm 1833.59 \mu\text{S/cm}$ ) and TDS ( $\pm 1079.1 \text{ mg/l}$ ). The

**Table 1** Range of analyzed groundwater and surface water samples compared to standards WHO (2004), in mg/l, EC in  $\mu\text{S}/\text{cm}$

Parameter	Groundwater				Surface water							WHO (2004)
	Minimum	Maximum	Standard deviation	Mean	El Maleh River			Dams		Lakes		
					P56	P67	P50	P52	P72	P79		
pH	6.83	8.31	0.27	7.32	8.25	8.07	7.68	7.26	9.96	10.17	6.5–8.5	
T°	17	25	0.3	22.17	17.10	15.90	17.00	17.00	27.50	25.00	–	
EC	811	8840	1833.59	4115.31	3490	5730	574	1462	14,650	39,400	1400	
Ca <sup>2+</sup>	24.32	307.6	65.4	140.62	170.54	194.14	54.97	84.02	117.12	199.68	75	
Mg <sup>2+</sup>	6.56	348.85	74.84	141.87	127.01	144.36	25.83	56.77	329.25	488.10	50	
Na <sup>+</sup>	36.87	1715.01	288.61	480.73	414.31	801.37	51.38	151.78	2522.27	8374.85	200	
K <sup>+</sup>	0.2	27.21	4.27	4.12	7.68	8.34	5.13	7.89	63.23	54.92	55	
HCO <sub>3</sub> <sup>-</sup>	97.6	677.21	95.94	322.52	328.18	389.18	163.48	231.80	187.88	107.36	300	
Cl <sup>-</sup>	120.7	2527.72	594.12	1114.56	893.32	1611.20	133.43	324.91	4760.41	13,597.37	250	
SO <sub>4</sub> <sup>2-</sup>	17.56	436.46	86.97	164.82	281.95	320.80	40.10	92.59	863.27	2054.99	400	
NO <sub>3</sub> <sup>-</sup>	5.94	288.31	61.9	73.92	23.21	52.02	6.86	18.48	0.00	0.00	50	
TDS	425.43	5322.35	1079.1	2452.25	2246.20	3521.41	481.17	968.24	8843.43	24,877.27	1000	
TH	231.67	2204.6	457.91	935.13	948.1678	1078.4	243.44	443.227	1647.1	2506.7	100	
SI of anhydrite	- 2.46	- 1.27	0.29	- 1.81	-	-	-	-	-	-	-	
SI of aragonite	- 0.51	0.65	0.26	0.04	-	-	-	-	-	-	-	
SI of calcite	- 0.37	0.79	0.26	0.18	-	-	-	-	-	-	-	
SI of dolomite	- 1.46	1.89	0.6	0.66	-	-	-	-	-	-	-	
SI of gypsum	- 2.23	- 1.05	0.29	- 1.59	-	-	-	-	-	-	-	
SI of Halite	- 6.90	- 4.09	0.57	- 5.09	-	-	-	-	-	-	-	
pCO <sub>2</sub> (10 <sup>-2</sup> atm)	7.21	26.45	4.41	15.25	-	-	-	-	-	-	-	
<sup>18</sup> O (‰)	- 4.55	- 2.66	0.53	- 3.73	- 2.97	- 2.26	- 6.27	- 2.74	1.53	0.32	-	
<sup>2</sup> H (‰)	- 28.53	- 15.85	3.44	- 22.81	- 18.4	- 13.65	- 37.41	- 18.48	8.35	1.29	-	
Precipitation												
<sup>18</sup> O (‰)	- 5.97	- 1.51	1.14	- 3.83	-	-	-	-	-	-	-	
<sup>2</sup> H (‰)	- 35.55	- 2.60	9.17	- 19.69	-	-	-	-	-	-	-	
d-Excess (‰)	6.87	15.05	2.23	10.92	-	-	-	-	-	-	-	

electrical conductivity of groundwater also varies considerably from 811 to 8840  $\mu\text{S}/\text{cm}$  (average of 4115.31  $\mu\text{S}/\text{cm}$ ). Likewise, TDS ranged from 425 to 5322.35 mg/l (average of 2452.25 mg/l). Most of the major cations ( $\text{Na}^+$ ,  $\text{Ca}^{2+}$ ,  $\text{Mg}^{2+}$ ) are all high with mean concentrations of 480.73, 140.62, 141.87 mg/l respectively, while potassium has a mean concentration of 4.12 mg/L. Similarly, most of the major anions ( $\text{Cl}^-$ ,  $\text{HCO}_3^-$  and  $\text{NO}_3^-$  but not  $\text{SO}_4^{2-}$ ) are also high with mean concentrations of 1114.56, 322.27, 82.92 and 156.31 mg/l, respectively. Overall, the general dominance of cations and anions goes in the order of  $\text{Na}^+ > \text{Mg}^{2+} > \text{Ca}^{2+} > \text{K}^+$  and  $\text{Cl}^- > \text{HCO}_3^- > \text{SO}_4^{2-} > \text{NO}_3^-$ , respectively. Except for sulfate and potassium, the concentrations of all other chemical components significantly exceed the maximum permissible limits set by the WHO (2004).

The pH values of the surface water show significant variation according to the type of water catchment. For example, the waters from the dams have a neutral pH with an alkaline tendency (pH of 7.26 and 7.68), while the waters of the El Maleh River (pH of 8.05 and 8.25) and lake waters (pH = 9.96 and 10.17) have basic pH values. The water temperature shows a clear variation. It ranges from 15.90 to 17.10 °C when measured along the El Maleh River and in the waters of the two dams, and from 25 to 27.50 °C when measured in the lakes. The electrical conductivity (EC) (Table 1) measured in surface water varies from 574 to 1462  $\mu\text{S}/\text{cm}$  when measured in the waters of the Mazer (p50) and the El Haimer dams (p52), respectively. The highest values were recorded along the El Maled River (between 3490 and 5730  $\mu\text{S}/\text{cm}$ ). The highest EC values were those measured in the waters of the two lakes (p72's EC is 14,650  $\mu\text{S}/\text{cm}$  and p79's is 39,400  $\mu\text{S}/\text{cm}$ ), with the latter EC value being similar to that of seawater. Thus, the temperature and EC values of the waters from the El Maleh River and the dams are close to the averages of these three groundwater parameters.

As per TDS classification (Fig. 2), only 12.68% of points have water with a TDS < 1000 mg/l and are natural freshwater, mostly originated in the intakes zones within the southern and northern Cenomanian regions, which is mostly composed of marls and limestone. Some 25.35% of points have a TDS greater than 3000 mg/l, meaning they are classified as very hard-brackish. These samples came from Primary and Triassic deposits primarily composed of shale and quartzite in the extreme east and west, respectively. Nonetheless, as shown in Fig. 2, approximately 62% of groundwater samples have a TDS in the range of 1000–3000 mg/l, demonstrating the hard brackish water of the Pliocene–Quaternary aquifer, which was the result of mixing the groundwater of the two previous aquifers (Freeze and Cherry 1979; Fetter 1990). In terms of TH classification, all samples exceed the maximum permissible limit (100 mg  $\text{CaCO}_3/\text{l}$ ) set by the WHO (2004),

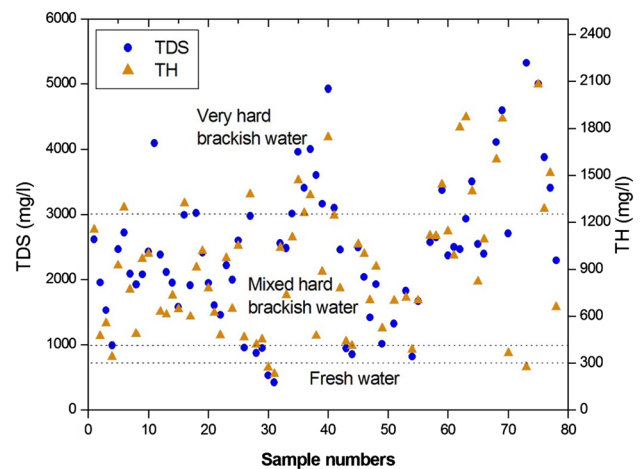


Fig. 2 TDS and TH classification

and almost all groundwater samples are above 300 mg  $\text{CaCO}_3/\text{l}$ , meaning they are in the category of hard and very hard waters, with only 2 samples (p30 and p31) being classed as natural freshwater (< 300 mg  $\text{CaCO}_3/\text{l}$ ) (Sawyer et al. 2003).

As discussed earlier, when moving from the west to the center of the plain, groundwater flows through Primary shale, Triassic and Infra-Cenomanian clay, Cenomanian limestone marl, and finally the sandstone of the Pliocene and Quaternary. These layers go in the reverse order, with the exception of Primary toward the EL Mellah River. Similarly, the spatial distribution of TDS (Fig. 3) shows that it increases from 900 mg/l in the high topographic areas in the south to 2400 mg/l in the north, with a complete coincidence with the regional groundwater flow. This gradual increase in TDS provides evidence of a significant lateral input of freshwater from the Phosphate Plateau, which dilutes the groundwater mineralization and participates in this recharge of the Berrechid aquifer. In contrast, the higher concentrations of TDS are located in the eastern and western parts of the plain. In addition, the sharp drop in TDS value from 2400 to 400 mg/l to the north of Mediouna reflects probably the low groundwater flow in this zone. These results perfectly concur with those of Hazan and Moullard (1962), who suggested that samples from the Primary, Triassic, and Cenomanian areas located in the east and west correspond to saltwater, while samples from the Pliocene and Quaternary areas in the north, center, and south of the plain correspond to freshwater, regardless of the distance travelled. In general, it becomes apparent that upstream of the basin in the south, the groundwater quality is appropriate for any purpose, but quality degrades downstream toward the central parts and the borders.

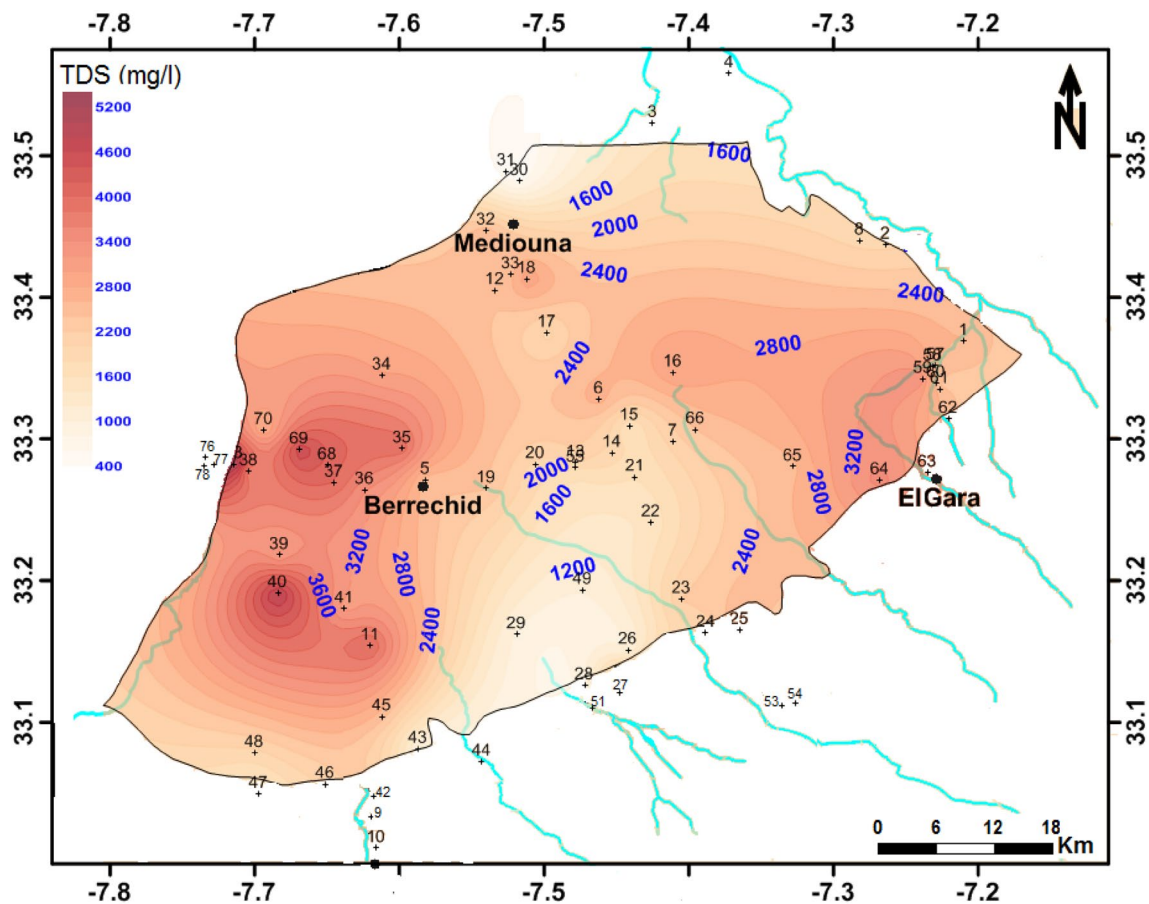


Fig. 3 Iso-concentration map of TDS (mg/l)

### Water type

To better illustrate the different chemical composition of the groundwater in the Berrechid aquifer, chemical data is plotted in a Piper diagram (Fig. 4). This allowed distinguishing between three main water types for groundwater:

1. Ca–Mg–HCO<sub>3</sub>–Cl, representing the low mineralization waters circulating in the Cenomanian formations located to the south of the Phosphate Plateau and north, downstream of the basin;
2. Mixed Na–Mg–Ca–Cl, corresponding to the waters circulating in the Cenomanian and Plio-Quaternary aquifers in the central portion of the basin; and
3. Na–Cl, representing the waters with the highest mineralization due to their circulation in the Primary, Permo-Triassic, and Infra-Cenomanian formations encountered at the points located to the east and west of the study area.

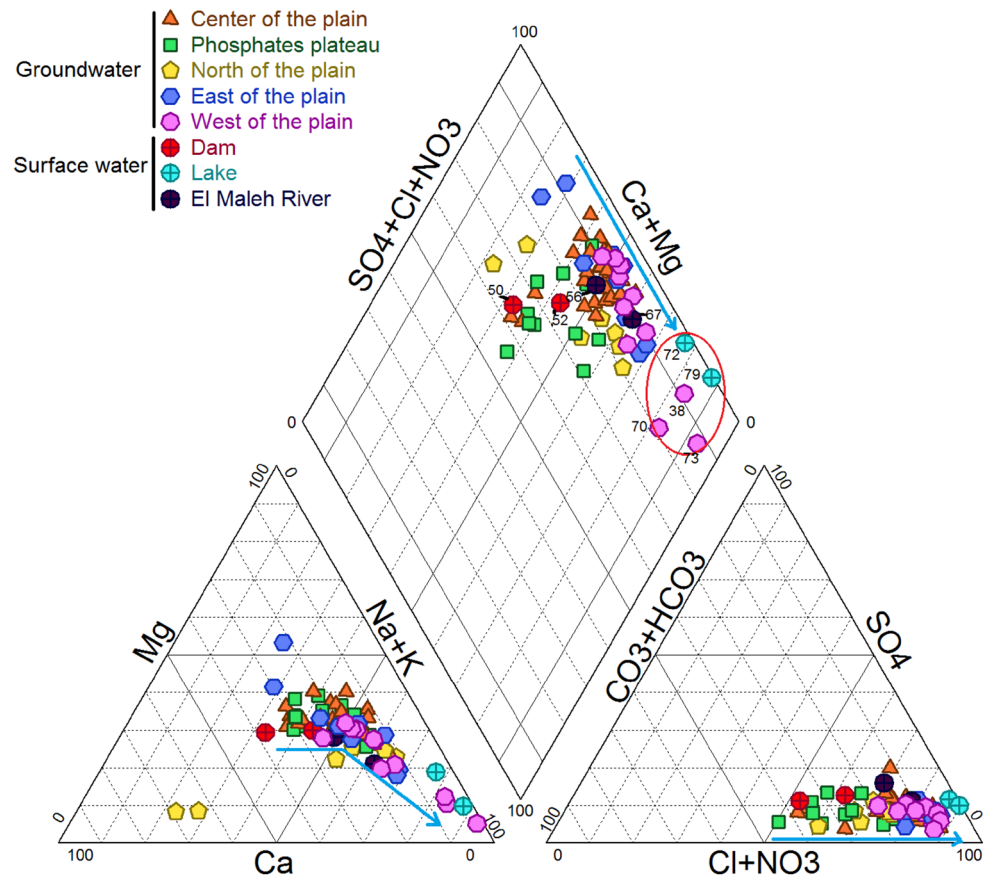
Nevertheless, it seems that almost all groundwater samples fell into the last two water types. Moreover, the transition

of waters from Ca–Mg–HCO<sub>3</sub>–Cl and Na–Mg–Ca–Cl toward Na–Cl type without an increment in the percentage of Cl<sup>–</sup> indicates the adsorption of Na<sup>+</sup>.

The chemical composition of surface water in the piper diagram shows significant variation. Indeed, the waters of the two dams (p50 and p52) are distributed between the first two facies, thus reflecting a predominant meteoric contribution supported by anthropogenic influence. The samples from the two lakes (p72 and p79) are plotted very close to the p38, p70 and p73 samples, having sodium chloride facies. On one hand, this indicates an intense evaporation and/or alteration of the silicate rocks (the Primary scales and quartz). On the other hand, meanwhile, it could well indicate the interconnection between the waters of these lakes and the groundwater in the region. The samples from the El Maleh River appear in the diagram next to the groundwater samples, and its evolution from Na–Mg–Ca–Cl (p56) to Na–Cl (p67) display enrichment in the chemical composition of the river's water, indicating the existence of a mixture with the groundwater provided by the dispersed springs along the northeastern part of the plain. On the basis of these results, and inasmuch the study



Fig. 4 Piper diagram



area is characterized by a semi-arid climate, low permeability values mainly in the borders, and by a mineralogical composition rich in carbonate and evaporate rocks, an initial approximation leads one to suspect that evaporation, the weathering of rocks, and cation exchange contribute to the groundwater's chemical evolution in the study area.

### Saturation indexes

The calculated values of saturation index (SI) for carbonate minerals; aragonite, calcite, and dolomite (Table 1, Fig. 5), range from  $-0.51$  to  $0.65$ ,  $-0.37$  to  $0.79$ , and  $-1.46$  to  $1.89$ , with averages of  $0.04$ ,  $0.18$  and  $0.66$  respectively. Average SI values show that carbonate minerals are thermodynamically oversaturated in the groundwater samples from the border areas in the east and the west, and they are near saturated in the samples from the rest of the plain, indicating that precipitation is expected for these minerals. In contrast, all of the groundwater samples are below the equilibrium for anhydrite ( $-2.46 \leq SI \leq -1.27$ ), gypsum ( $-2.23 \leq SI \leq -1.05$ ), and halite ( $-6.9 \leq SI \leq -4.24$ ), suggesting that these evaporate minerals are expected to dissolve.

### Correlation matrix

Pearson's correlation matrix was applied to describe the relationships between two or more chemical parameters. The interpretation of the dataset was accomplished by considering component loadings more than  $r^2 = 0.6$ . When referring to absolute coefficient values less than  $0.5$ ,  $0.5$ – $0.6$ ,  $0.60$ – $0.75$  and greater than  $0.75$ , the correlations are described using the words "weak," "modest," "good," and "strong," respectively. The significance of correlation coefficients was tested at alpha level  $p < 0.05$  for the samples ( $n = 71$ ). In this study, the correlation matrix was calculated using the XlStat software. The results (see Table 2) show how TDS is highly correlated with the concentrations of  $\text{Cl}^-$  ( $0.99$ ),  $\text{Na}^+$  ( $0.91$ ),  $\text{SO}_4^{2-}$  ( $0.81$ ),  $\text{Mg}^{2+}$  ( $0.76$ ), and  $\text{Ca}^{2+}$  ( $0.62$ ), indicating that a high level of groundwater mineralization is related to the dissolution of these ions.

### Identification of hydrogeochemical processes

The unequal distribution of salinity appears to originate from many factors, and this probably reflects the heterogeneity of the Berrechid aquifer, as well as the impact of varying environmental conditions. The chemical characteristic of the

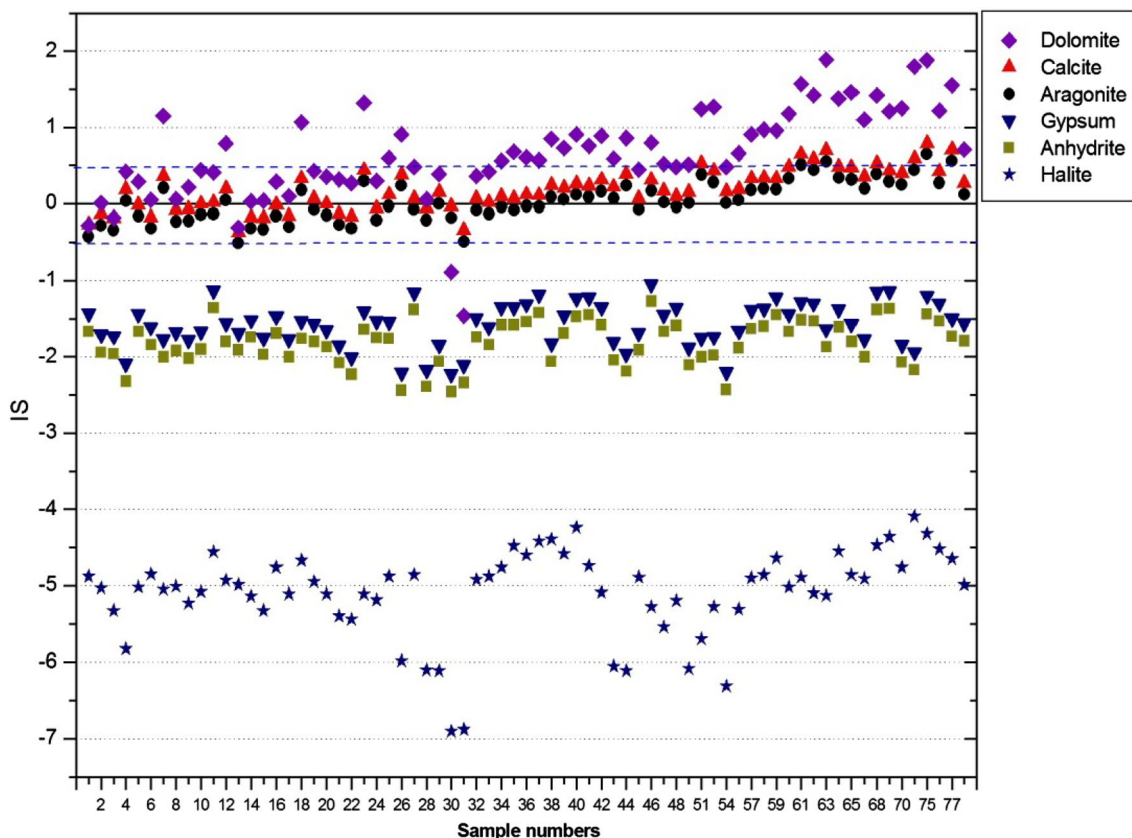


Fig. 5 Saturation indexes of groundwater samples

Table 2 Pearson’s correlation matrix for hydrochemical parameters at the probability of 95%

	$T (^{\circ}C)$	pH	TDS	$Ca^{2+}$	$Mg^{2+}$	$Na^{+}$	$K^{+}$	$HCO_3^{-}$	$Cl^{-}$	$SO_4^{2-}$	$NO_3^{-}$	$pCO_2$
$T (^{\circ}C)$	1											
pH	-0.42	1										
TDS	-0.31	0.12	1									
$Ca^{2+}$	-0.23	-0.13	<b>0.62</b>	1								
$Mg^{2+}$	-0.19	-0.13	<b>0.76</b>	<b>0.88</b>	1							
$Na^{+}$	-0.35	0.3	<b>0.91</b>	0.29	0.45	1						
$K^{+}$	-0.18	0.45	0.27	-0.02	0.02	0.37	1					
$HCO_3^{-}$	-0.29	0.13	0.29	-0.11	0.09	0.42	0.32	1				
$Cl^{-}$	-0.31	0.11	<b>0.99</b>	<b>0.66</b>	<b>0.79</b>	<b>0.88</b>	0.25	0.20	1			
$SO_4^{2-}$	-0.15	0.13	<b>0.81</b>	0.42	0.54	<b>0.79</b>	0.27	0.38	<b>0.77</b>	1		
$NO_3^{-}$	-0.195	0.12	0.26	0.43	0.39	0.12	0.12	0.06	0.21	0.07	1	
$pCO_2$	0.315	- <b>0.88</b>	-0.03	0.01	0.10	-0.13	-0.27	0.33	-0.07	0.02	-0.11	1

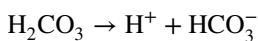
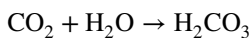
Values in bold indicate significant correlations (correlation coefficient > 0.6) at the 0.05 level

groundwater is generally related to the concentration of its different constituents. In turn, the concentrations of these species depend on their availability in the rocks. Climatic conditions, lithology, geological formations, carbon dioxide, salt solubility, and anthropogenic activities all play important roles in the chemical evolution of groundwater (Appelo and Postma 1993; Lakshmanan et al. 2003).

Water moving through the aquifer during infiltration and residence reacts quite readily with sedimentary rock, and since carbonates are present in these rocks, their concentration in water is mostly related to the interaction between water and these carbonate rocks. The limestone, sandstone, marble, shale and even some carbonate rocks make up the main sources of carbonate in the study area. The results of

the geochemical modeling study conducted by El Ghali et al. (2018a) using NETPATH program along the regional flow-path in the Berrechid aquifer, have shown that from the south to the center of the open conditions system, the dedolomitization process (dolomite dissolution and calcite precipitation driven by gypsum dissolution), dissolution of halite and cation exchange are strongly be in charge of the mineralization of groundwater, and further to the north in downstream area where  $\text{CO}_2$  gas was consumed, the previous reactions are fully reversed for calcite dissolution and precipitation of gypsum and dolomite, probably indicating, low water flow and differences in recharge water composition in this zone.

The strong negative correlation ( $-0.88$ ) between pH and the partial pressure of carbon dioxide ( $\text{pCO}_2$ ) indicate the natural dependence of these properties. The  $\text{pCO}_2$  values range between  $7.21 \times 10^{-2}$  and  $26.45 \times 10^{-2}$  atm, and they are generally greater than the value of atmospheric  $\text{CO}_2$  ( $0.039 \times 10^{-2}$  atm) (Van der Weijden and Pacheco 2003). This indicates that groundwater has acquired excess  $\text{CO}_2$  from atmospheric  $\text{CO}_2$ , the deterioration of organic soil matter, and vegetative root activity (Subba Rao 2002). In turn, the interaction between  $\text{CO}_2$  and water forms a weak carbonic acid ( $\text{H}_2\text{CO}_3$ ), which then dissociates into hydrogen and bicarbonate as explained below.



The groundwater of the study area demonstrates a good relationship between calcium and magnesium (0.88), suggesting common sources for these elements. Datta and Tyagi (1996) explained that if  $\text{Ca}^{2+}$  and  $\text{Mg}^{2+}$  in the system only originate from the dissolution of carbonate and evaporate minerals, the points will fall along the equiline

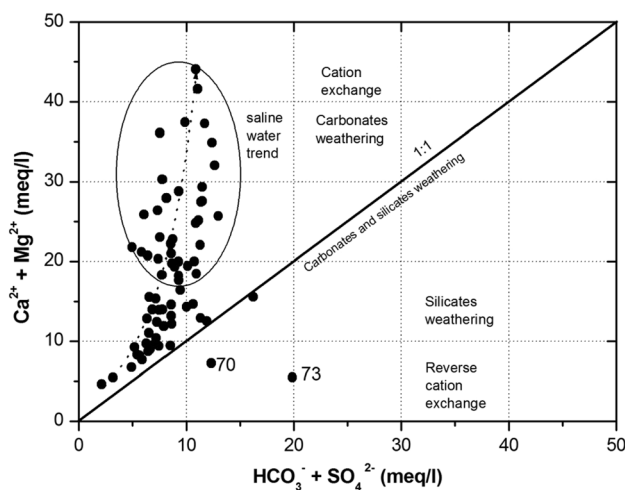


Fig. 6  $(\text{Ca}^{2+} + \text{Mg}^{2+})$  vs.  $(\text{HCO}_3^- + \text{SO}_4^{2-})$

(1:1) in the  $(\text{Ca}^{2+} + \text{Mg}^{2+})$  versus  $(\text{HCO}_3^- + \text{SO}_4^{2-})$  scatter diagram. However, the data for the study area as plotted in Fig. 6 shows that almost all of the samples' points lie far above the equiline (1:1). Only two samples (p70 and p73) lie below the equiline, and these probably derive from silicate weathering and/or reverse cation exchange. This clearly indicates that the calcium and magnesium ions in groundwater are not derived solely from the weathering of carbonate rocks. Therefore, the large excess of  $(\text{Ca}^{2+} + \text{Mg}^{2+})$  over  $(\text{HCO}_3^- + \text{SO}_4^{2-})$  can be thought of as being related to other processes, such as cation exchange again (Lakshmanan et al. 2003; Rajmohan and Elango 2004; Bozdağ 2016). In addition, despite carbonate rock being abundant in the aquifer,  $\text{HCO}_3^-$  is not the major anion in the groundwater and displays a weak correlation with  $\text{Ca}^{2+}$  ( $-0.11$ ) and  $\text{Mg}^{2+}$  ( $0.09$ ) indicating that carbonates have been balanced out by alkalis ( $\text{Na}^+$  and  $\text{K}^+$ ) (Singh and Hasnain 1999; Subba Rao 2002; Kumar et al. 2006) and thus reflect the presence of an additional source of  $\text{Ca}^{2+}$  and  $\text{Mg}^{2+}$  such as cation exchange.

Again, if  $\text{Ca}^{2+}$  and  $\text{Mg}^{2+}$  result only from carbonate weathering and dissolution, the ionic concentrations should be close to the slope 0.5 in a plot of  $m(\text{Ca}^{2+} + \text{Mg}^{2+})$  versus  $m(\text{HCO}_3^-)$  (Sami 1992). Nonetheless, all the samples used in the present study lie above this slope (Fig. 7). Therefore, the high ratios of  $\text{Ca}^{2+}$  and  $\text{Mg}^{2+}$  cannot be related primarily to carbonate weathering, nor can they be explained by the consumption of  $\text{HCO}_3^-$  in the formation of carbonic acid ( $\text{H}_2\text{CO}_3$ ), because this cannot form under existing basic conditions (Spears 1986). In addition, it is also important to observe in Fig. 6 the noticeable trend toward increasing the  $(\text{Ca}^{2+} + \text{Mg}^{2+})$  content, which is mostly prominent in groundwater collected from wells located in the eastern and western parts characterized by low permeability. These highly saline groundwater with TDS greater than 3000 mg/l were classified as very hard brackish water (Fig. 2) and are

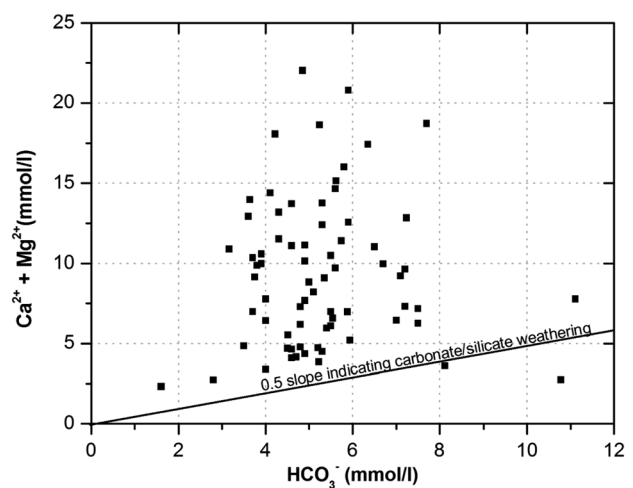


Fig. 7  $(\text{Ca}^{2+} + \text{Mg}^{2+})$  vs.  $\text{HCO}_3^-$



thermodynamically supersaturated with respect to carbonate minerals (aragonite, calcite, and dolomite). Hence, to explain the observed trend, many factors are considered; groundwater circulation through the dolomitic limestone-rich formations in these areas, the potential water–rock interactions in cation-exchange reactions through the liberation of exchangeable cations ( $\text{Ca}^{2+}$  and  $\text{Mg}^{2+}$ ) previously fixed to the surface of the aquifer’s clay minerals and the retention of  $\text{Na}^+$  present in the water, and the concentration of recycled irrigation water constituents during evaporation (see below).

Although sulfate is strongly correlated with  $\text{Na}^+$  (0.79) and TDS (0.81) (Table 2), its concentration in the groundwater is feeble, reflecting presumably a weak dissolution of sulfate and evaporate minerals [weak correlation between  $\text{Ca}^{2+}$  and  $\text{SO}_4^{2-}$  (0.42)]. Furthermore, the graph of  $\text{Ca}^{2+}$  versus  $\text{SO}_4^{2-}$  (Fig. 8) shows that most of the groundwater samples points plot above the gypsum dissolution line and point to  $\text{Ca}^{2+}$  enrichment or significant removal of  $\text{SO}_4^{2-}$  from the groundwater system. The excess of calcium behavior over sulfate is particularly a significant indication for additional geochemical processes such as cation exchange reactions of  $\text{Ca}^{2+}$  with  $\text{Na}^+$  and dissolution of other evaporites association’s minerals like calcium chloride (a good correlation (0.66) between  $\text{Ca}^{2+}$  and  $\text{Cl}^-$ ). Gypsum precipitation cannot be considered as an explanation for sulfate deficiency as SI gypsum values are quite negative in all groundwater samples (Fig. 5). However, the lower ratios of  $\text{SO}_4^{2-}/\text{Cl}^-$  in all samples let expecting to be related to sulfate reduction. Similar behavior was reported by (Datta and Tyagi 1996), where groundwater is characterized by higher chloride concentrations and low sulfate content.

The predominant chloride and sodium elements in groundwater samples are strongly correlated (0.88) to each other and are strongly correlated with TDS, with values of

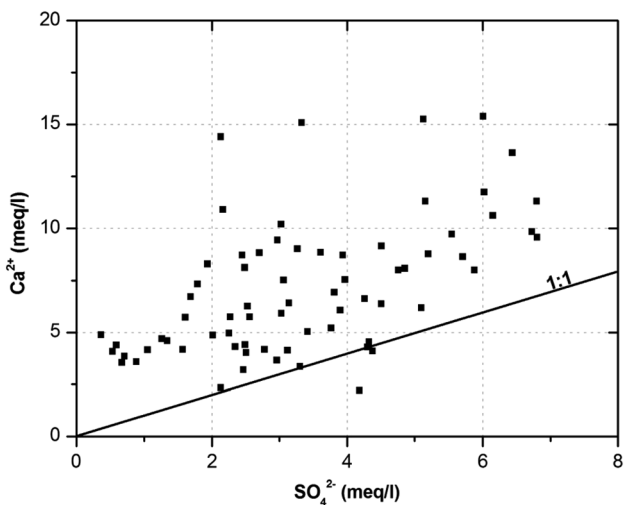


Fig. 8  $\text{Ca}^{2+}$  vs.  $\text{SO}_4^{2-}$

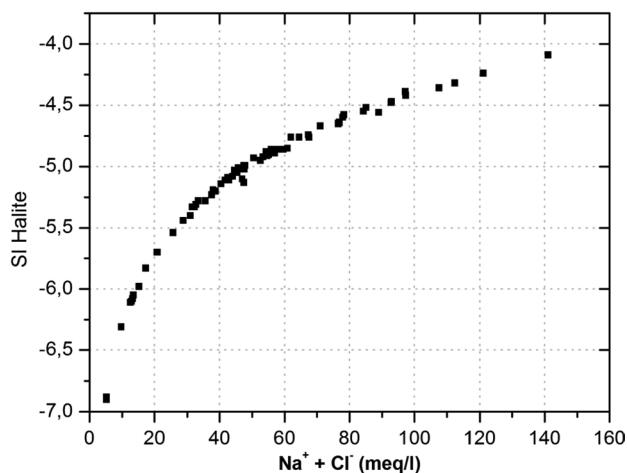


Fig. 9 SI halite vs  $(\text{Na}^+ + \text{Cl}^-)$

0.98 and 0.91, respectively. As shown in Fig. 9, the inverse parabolic correlation between  $(\text{Na}^+ + \text{Cl}^-)$  and the negative saturation indexes of halite suggest that halite dissolution could be a common source of these elements. In addition, compared to the other evaporate minerals anhydrite and gypsum, halite present the most undersaturated state, indicating that halite dissolution can undergo an important role in the chemical evolution of the groundwater. If chloride and sodium are derived from halite dissolution, the  $\text{Na}^+/\text{Cl}^-$  molar ratio should be equal to 1. However, the  $\text{Na}^+/\text{Cl}^-$  relationship (Fig. 10), shows that the majority of samples fall above the 1:1 ( $\text{Na}:\text{Cl}$ ) line, and the average ratio of  $\text{Na}^+/\text{Cl}^-$  in the study area is 0.67, which is lower than the expected dissolution of halite highlighting thereby, a disequilibrium and a divergence to more chloride, caused either by excess of chloride and/or the depletion of sodium. The silicate weathering marked by high levels of  $\text{Na}^+$  and

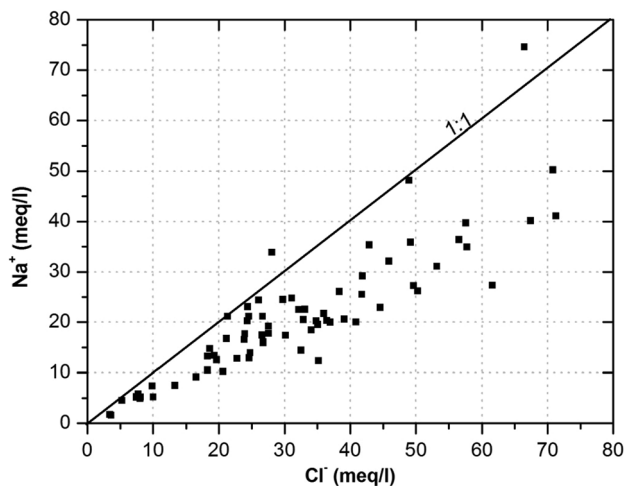


Fig. 10  $\text{Na}^+$  vs  $\text{Cl}^-$

HCO<sub>3</sub><sup>-</sup> in the two samples p70 and p73 lying below the halite dissolution line, cannot be a major source of all groundwater samples since HCO<sub>3</sub><sup>-</sup> is not the dominant anion in groundwater of the study area. As result, higher concentrations of Cl<sup>-</sup> and depletion of Na<sup>+</sup> suggest further modification during water circulation, such as the long history of evapotranspiration, cation exchange, the mixing of freshwater with saline water, rock salt dissolution, and agricultural contamination (Datta and Tyagi 1996).

For better determination of the prevailing hydrochemical processes controlling the groundwater chemistry, Gibbs diagram (Gibbs 1970) was created by plotting the ratios of Na<sup>+</sup> to (Na<sup>+</sup> + Ca<sup>2+</sup>) and Cl<sup>-</sup> to (Cl<sup>-</sup> + HCO<sub>3</sub><sup>-</sup>) against TDS. Figure 11 shows that almost all of the groundwater samples fall into the evaporation zone, and only a few groundwater samples are in the zone of rock weathering, implying that evaporation is the principal control of groundwater chemistry in the study area. Evaporation greatly increases the concentration of ions and deposition of evaporites that are eventually leached into the saturated zone leading to high salinity and TDS. Its effect is manifested in several significant relationship discussed throughout the following sections. For example, the relationship between Na<sup>+</sup>/Cl<sup>-</sup> and the electrical conductivity (Fig. 12), shows an almost horizontal line, which would be a substantial indicator of ion concentration by evaporation (Jankowski and Acworth 1997).

It is usually known that in typical areas under semi-arid conditions, leaching of saline soil residues into the groundwater system is a common source of Na<sup>+</sup>, K<sup>+</sup>, Cl<sup>-</sup>, and SO<sub>4</sub><sup>2-</sup> ions (Datta and Tyagi 1996; Srinivasamoorthy et al. 2011; Bozdağ 2016). This is, indeed, the case in Fig. 13 which demonstrates that the concentrations of (Na<sup>+</sup> + K<sup>+</sup>) and (Cl<sup>-</sup> + SO<sub>4</sub><sup>2-</sup>) in the sampled points

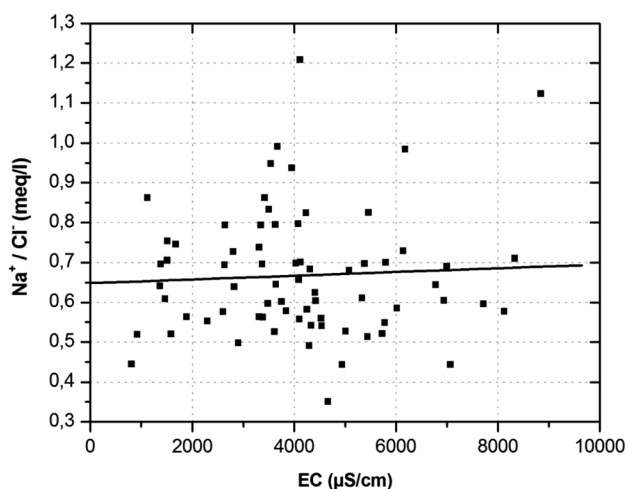
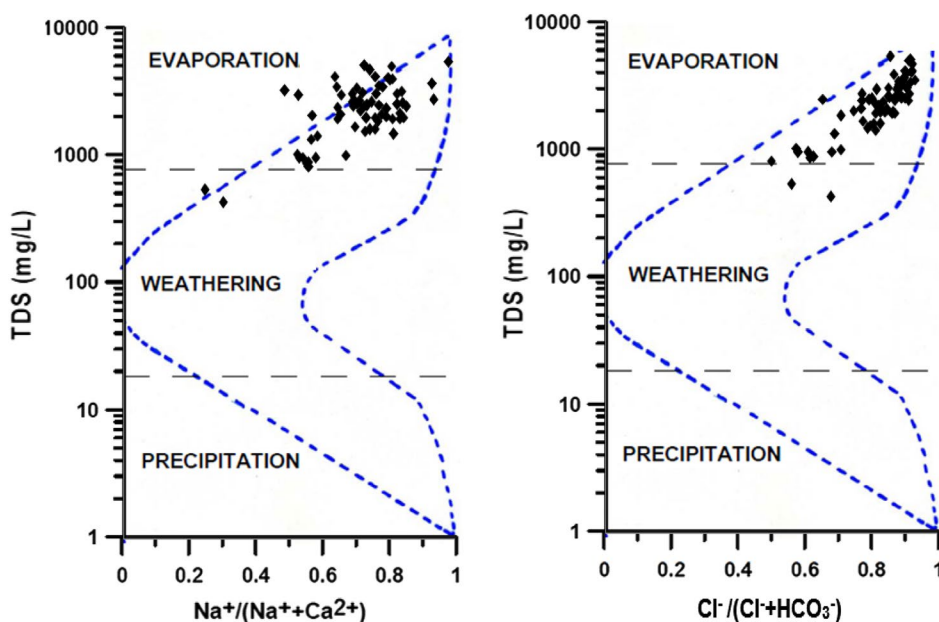


Fig. 12 Na<sup>+</sup>/Cl<sup>-</sup> vs EC

increase simultaneously. Furthermore, the lower ratios of SO<sub>4</sub><sup>2-</sup>/Cl<sup>-</sup> ranging between 0.05 and 0.3, indicating the application of gypsum fertilizers (Rajmohan and Elango 2006). The application of fertilizers in the study area in the form of (NH<sub>4</sub>)<sub>2</sub>SO<sub>4</sub> and MgSO<sub>4</sub> is also highlighted by the modest correlation between Mg<sup>2+</sup> and SO<sub>4</sub><sup>2-</sup> (0.54). In addition, the chloride ion in wind-driven aerosols may be absorbed in the atmosphere by rainwater and released into the groundwater, thereby increasing the excess of chloride in the groundwater. Salama et al. (1993) explain that during the dry period or in low-rainfall areas, aerosol salts and dissolved salts in the subsoil are concentrated by water uptake by plant roots (salt input exceeds salt output). These are then transported into the deeper formations by water recharging the system. Then, during a wet period, a

Fig. 11 Plots of the major ions within the Gibbs boomerang envelope (the blue lines) for groundwater in the Berrechid basin



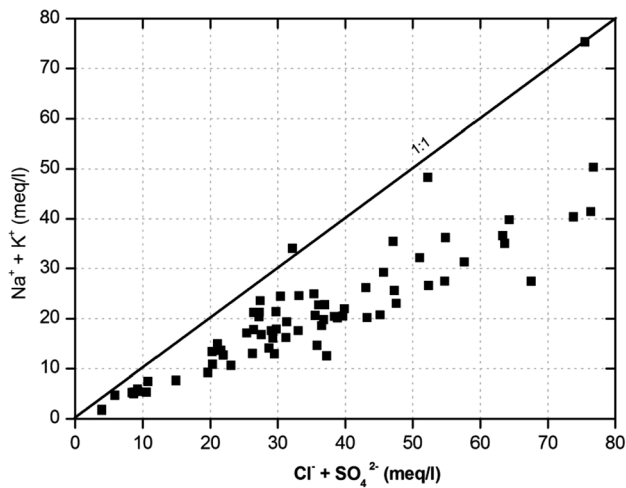


Fig. 13  $(\text{Na}^+ + \text{K}^+)$  vs.  $(\text{Cl}^- + \text{SO}_4^{2-})$

dissolution of salt-like halite (NaCl) and magnesium chloride hydrate ( $\text{MgCl}_2 \cdot \text{MgCO}_3$ ) occurs, facilitating the downward movement of  $\text{Na}^+$  and  $\text{Cl}^-$  along desiccation cracks in the upper soil (Jankowski and Acworth 1997). Consequently, the enrichment of groundwater with  $\text{Cl}^-$  and  $\text{Na}^+$  could be caused by evaporation, the dissolution of halite, the leaching of soil salt and anthropogenic activities.

The modest concentration of potassium in the groundwater may be ascribed to its low geochemical versatility due to the resistance of rocks containing  $\text{K}^+$  (feldspars and illite) to chemical weathering and its tendency to be reincorporated into weathering solid products especially clay minerals (García et al. 2001; Al-Charideh and Abou-Zakhem 2010). Significant potassium values in the waters of the Berrechid basin are namely recorded in the western part of the basin, whether in groundwater (8.56 to 27.21 mg/l) or in lake waters (11.38 to 63.23 mg/l) circulating in the Primary formations (schists and quartzite). These high concentrations are mainly due to the dissolution processes of potassium-containing silicate minerals (K-feldspar) and reverse cation exchange previously noted in both p70 and p73 samples.

The excess observed for  $\text{Ca}^{2+}$  and  $\text{Mg}^{2+}$  in the groundwater versus  $\text{HCO}_3^-$  and  $\text{SO}_4^{2-}$  (see Fig. 6) and the relative excess of  $\text{Cl}^-$  with respect to  $\text{Na}^+$  clearly demonstrate the presence of a cation-exchange process (Salama et al. 1993; Rajmohan and Elango 2004; Zaidi et al. 2015). Evidence of a cation-exchange reaction is well shown on the Piper diagram (Fig. 4), with the line connecting the water composition changed by exchange starting parallel to constant magnesium and then moving down toward the sodium apex (Hounslow 1995). Cation-exchange reactions are considered an important geochemical process controlling the chemical composition of groundwater if, the relationship between  $((\text{Ca}^{2+} + \text{Mg}^{2+}) - (\text{HCO}_3^- - \text{SO}_4^{2-}))$  and  $((\text{Na}^+ + \text{K}^+) - \text{Cl}^-)$  is linear with a slope of  $-1$  (McLean et al. 2000). Figure 14

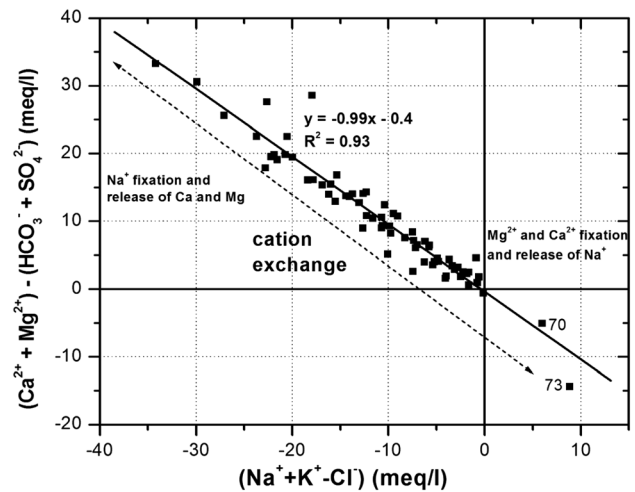
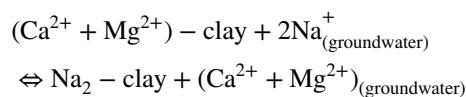


Fig. 14  $(\text{Ca}^{2+} + \text{Mg}^{2+}) - (\text{HCO}_3^- + \text{SO}_4^{2-})$  vs.  $(\text{Na}^+ + \text{K}^+ - \text{Cl}^-)$

shows that for data from the study area, this is close to being a straight line with a slope of  $(-0.99)$ , indicating an increase in  $(\text{Ca}^{2+} + \text{Mg}^{2+})$  related to a decrease in  $(\text{Na}^+ + \text{K}^+)$  or  $(\text{HCO}_3^- + \text{SO}_4^{2-})$  (García et al. 2001; Srinivasamoorthy et al. 2008; Bozdağ 2016). During cation-exchange reactions,  $\text{Na}^+$  present in the solution is eliminated and replaced by the exchangeable cations  $\text{Ca}^{2+}$  and  $\text{Mg}^{2+}$  fixed at the surface of clay minerals in the aquifer according to the following reaction (Salama et al. 1993).



This reaction reduces the concentration of  $\text{Na}^+$  and increases the concentrations of  $\text{Mg}^{2+}$  and  $\text{Ca}^{2+}$  in the

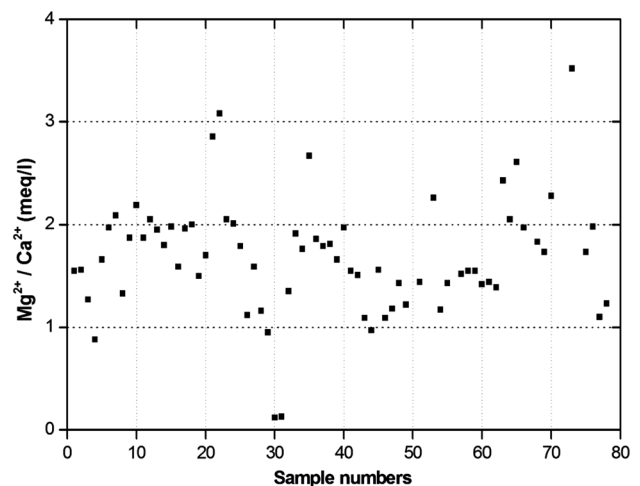


Fig. 15  $\text{Mg}^{2+}/\text{Ca}^{2+}$  ratio of groundwater samples

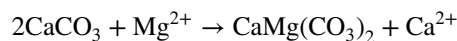


groundwater, except for the two p70 and p73 samples that originate from silicate weathering and a reverse cation exchange.

With the exception of the two samples p30 and p31 from calcite-limestone bedrock, Fig. 15 shows that most groundwater samples have higher ratios of  $Mg^{2+}/Ca^{2+}$ , ranging between 1 and 2 generally and exceeding 2 in some samples. Such ratios could be explained by the circulation of groundwater through the carbonate rock in the Berrechid basin demonstrated by the dedolomitization process shown in mass-transfer calculations (El Ghali et al. 2018a). During dedolomitization process, groundwater moving from recharge area to downgradient through the aquifer with a high concentration of  $CO_2$  and low dissolved solids content cause solution of calcite, dolomite and gypsum from the mineralogical framework. This result causes an increase in the total  $CO_2$  and increases in many of the other chemical constituents, particularly  $SO_4^{2-}$ ,  $Ca^{2+}$  and  $Mg^{2+}$ . When equilibrium with respect to calcite is reached,  $Ca^{2+}$  ions from the two sources and carbonate from dolomite combine to precipitate calcite. However, the groundwater is still undersaturated with respect to dolomite and gypsum and it continues to dissolve both of these minerals. As a result, the  $Ca^{2+}$  concentration decreases while the other constituents all continue to increase. Long residence times of water in such systems would produce  $Mg^{2+}/Ca^{2+}$  ratios above 1 and a high pH, with both tending to increase along the flow path. This continues until saturation with respect to dolomite occurs, at which time dolomite may precipitate concurrently with calcite. Higher  $Mg^{2+}/Ca^{2+}$  ratios could also be related to the cation exchange behavior of magnesium because during this process, the release of  $Mg^{2+}$  by aquifer material and adsorption of  $Na^+$  is more efficient than that of  $Ca^{2+}$  for  $Na^+$  (Salama et al. 1993). Another important origin of the higher  $Mg^{2+}/Ca^{2+}$  ratios is probably the mixing between freshwater and the more Mg-rich fluids that have encroached into the deeper parts of the aquifer. This idea is supported by considering the historical marine conditions of the study area marked by several periods of transgression and regression of the sea; under these conditions dolomitization may occur in the zones of brackish water (Hanshaw and Back 1979; Machel and Mountjoy 1986; Machel 2004).

The presence of such as conditions for dolomitization process in the eastern and western parts of the plain could be used to explain the oversaturation with aragonite, calcite and dolomite reported in samples located in these parts (Fig. 5), according to the following hydrodynamic model: The high level of  $CO_2$  dissolved in freshwater favors the dissolution of carbonate and evaporate minerals stored in different sedimentary rocks in the unsaturated zone. However, during the water's flow through the aquifer, the  $CO_2$  is used up and the

water becomes saturated with minerals, thereby permitting its direct precipitation (Subba Rao 2002). Moreover, cation-exchange reactions contribute much more to the rise in calcium and magnesium ion concentrations. In addition, the tectonic history of sedimentation in the study area together with the presence of some favorable thermodynamic conditions like a high evaporation rate, high ratios of  $Mg^{2+}/Ca^{2+}$  and a low concentration of  $SO_4^{2-}$  promote the precipitation of carbonate minerals. As result, dolomite formation occurs through a secondary replacement (dolomitization) of less soluble minerals (calcite and aragonite) that were previously precipitated according to the reaction below (Machel and Mountjoy 1986; Machel 2004):



### Nitrate water contamination

Nitrate concentration values in the groundwater samples show a wide variation from 5.94 to 288.31 mg/l, with an average of 73.92 mg/l (Table 1). Some 60% of the samples exceed the maximum limit normally expected in unpolluted water (50 mg/l) (WHO 2004). The spatial distribution of nitrate (Fig. 16) that with the exception of the recharge area in the south and following the flow direction toward the north, all areas of the plain contain high nitrate concentrations over the limit (50 mg/l), rising up to 100 mg/l close to the urban zones of cities. The examination of the nitrate distribution map (Fig. 16) indicates high levels that appear to be related to the impact of human activities. In fact, the implementation of large-scale flood irrigation in agricultural practices on the plain of Berrechid promotes the leaching of fertilizers and pesticides and their transport back to the aquifer through the infiltration of precipitation and irrigation flow return. The excessive enrichment of groundwater near urban areas, meanwhile, could be caused by direct infiltration from various sources of pollution, such as septic tanks, sewage effluent, and industrial waste (Fekri et al. 2012). El Bouqdaoui et al. (2009) explains that the undue nitrate concentration in the study area is particularly caused by an overuse of artificial fertilizers and industrial activities. Furthermore, this study's result is consistent with that found in the assessment of the Berrechid aquifer's vulnerability to pollution conducted by Ait Brahim et al. (2015) and Elfarrak et al. (2014) which report that the highest levels of vulnerability manifest in areas when water is shallow and in areas not protected by quaternary clays, specifically the southeast and northwest parts of the study area. These results should also support the idea of recharge through irrigation water return, which would likely have an evaporation enrichment signal.

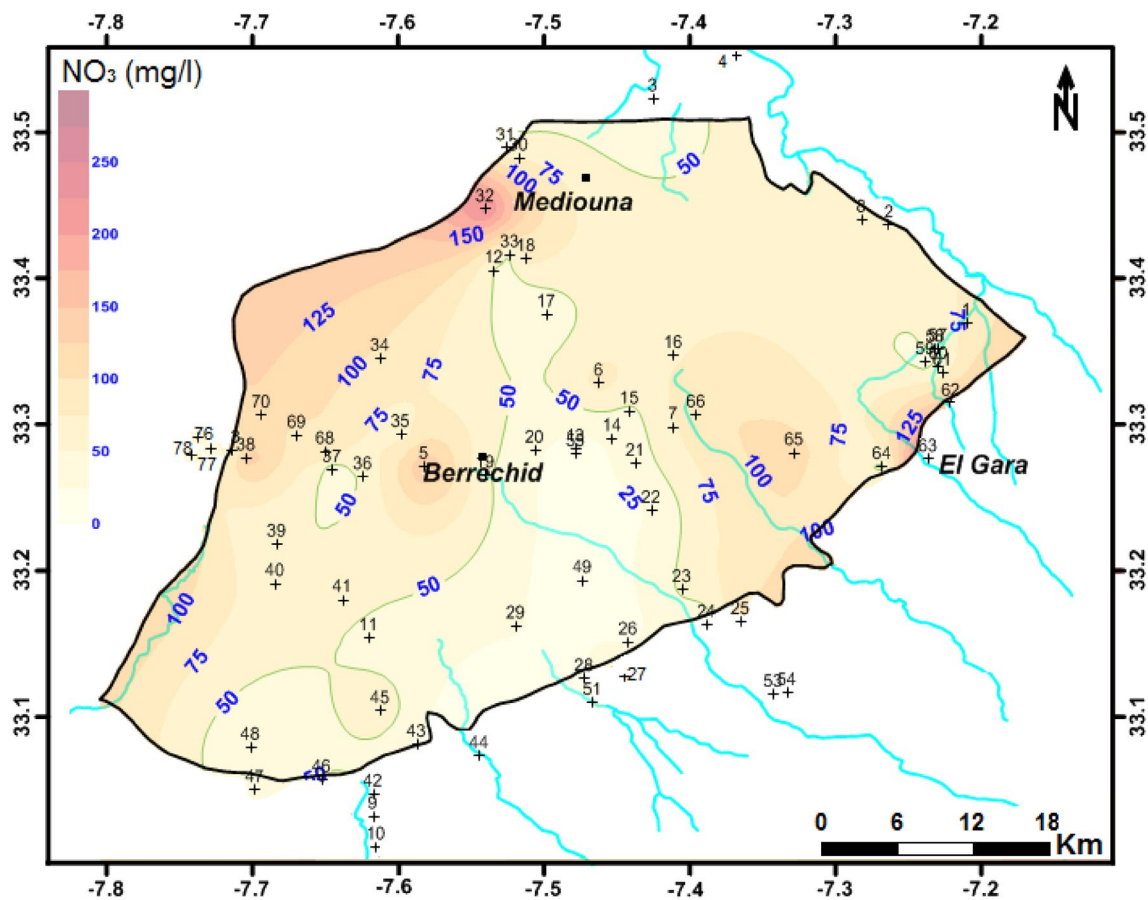


Fig. 16 Iso-concentration map of nitrate in mg/l

## Isotopic study

### Deuterium and oxygen-18

The environmental isotopes of oxygen-18 and deuterium are widely used in hydrology as natural tracers for elucidating water sources and flow paths, as well as to determine the hydrological processes influencing the chemical reactions occurring along hydrologic pathways, such as evaporation and mixing (Clark and Fritz 1997).

The isotopic composition of precipitation at six meteorological stations is described in Table 1 and plotted in Fig. 17. The  $\delta^{18}\text{O}$  values range from  $-5.97$  to  $-1.51\text{‰}$  and from  $-35.55$  to  $-2.60\text{‰}$  for  $\delta^2\text{H}$ . The data yields a Local Meteoric Water Line (LMWL) characterized by the equation:  $\delta^2\text{H} = 7.78 \delta^{18}\text{O} + 10.09$ ,  $R^2 = 0.94$  (El Ghali et al. 2018b). This line, which is characteristic of an Atlantic origin for the rains in the Berrechid basin, is very close to the Global Meteoric Line (GML:  $\delta^2\text{H} = 8.17 \delta^{18}\text{O} + 10.35$ ) (Rozanski et al. 1993) and the Regional Meteoric Water Line (RMWL:  $\delta^2\text{H} = 7.34 \delta^{18}\text{O} + 10.19$ ) defined by Ouda et al. (2005) from the daily rainfall measurements at the Rabat

station (located 100 km from Berrechid at an altitude of 75 m) (Fig. 17). Deuterium excess values were calculated as  $d = \delta^2\text{H} - 8 \delta^{18}\text{O}$  (Dansgaard 1964), and these vary from 6.87 to 15.05‰, with most values being higher than the average 10.92‰, indicating the attendance of the evaporation phenomenon imprint. Considering the fact that it is a semi-arid region with Atlantic-originating precipitation, the moderately high deuterium excess values denote a contribution of recycled continental water vapor and/or evaporated surface water to precipitation (Clark and Fritz 1997; Ouda et al. 2005; Marah et al. 2010).

The isotopic values of oxygen and deuterium for the 71 groundwater samples collected from the Berrechid aquifer (Table 1) range from  $-4.55$  to  $-2.66\text{‰}$  for  $\delta^{18}\text{O}$  and from  $-28.53$  to  $-15.85\text{‰}$  for  $\delta^2\text{H}$ . The regression results for  $\delta^{18}\text{O}$  and  $\delta^2\text{H}$  yielded an equation defined by  $\delta^2\text{H} = 5.83 \delta^{18}\text{O} - 1.064$  (Fig. 17). Therefore, in a comparison of the obtained values to the three meteoric water lines, the global  $\delta^2\text{H} = 8.17 \delta^{18}\text{O} + 10.35$  (Rozanski et al. 1993), the regional, and the local lines show most groundwater data points being plotted to the right, defining a single tendency with a slope of 5.83 and reflecting an evaporation slope of

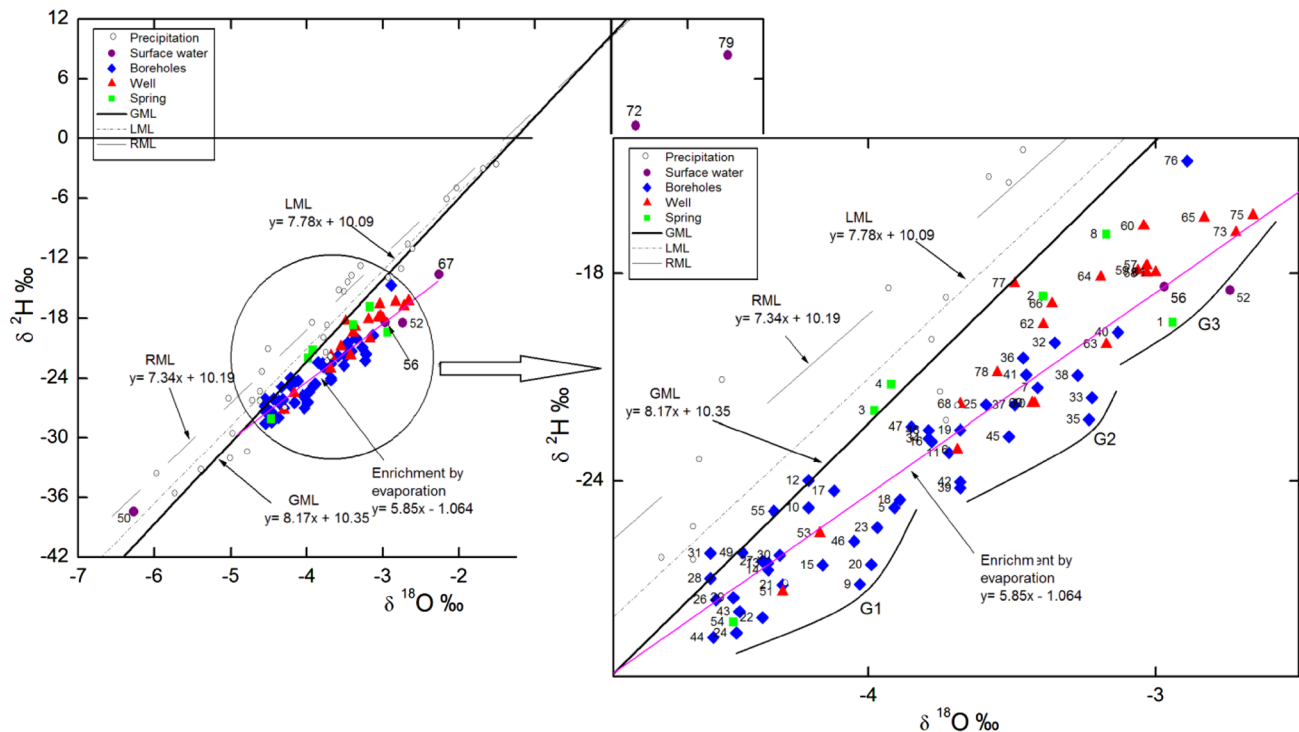


Fig. 17  $\delta^2\text{H}$  vs  $\delta^{18}\text{O}$

between 4 and 6 in semi-arid areas (Clark and Fritz 1997; Al-Charideh and Abou-Zakhem 2010; Srinivasamoorthy et al. 2011; Abderamane et al. 2013). However, a few samples located close to the LMWL and GMWL show an absence of evaporation phenomena, implying rapid infiltration of meteoric rainwater. Deviations from the three meteoric water lines suggest that evaporative enrichment has taken place for groundwater before recharge occurs. This suggests either raindrop evaporation before reaching the ground (Hoefs 1997), a delayed infiltration of precipitation in low permeability zones (the aquifer is covered by Quaternary alluvium consisting of very low permeability silt), and a mixing of meteoric water with evaporated water from rainfall, rivers, and irrigation return flow. The intersection of the evaporation line and the LMWL with values of  $-2.12$  for  $\delta^{18}\text{O}$  and  $-33.85\text{‰}$  for  $\delta^2\text{H}$  represents the initial isotopic composition of the groundwater before evaporation. Based on the locations the groundwater samples were taken from and the range of evaporation, an examination of the data plotted in Fig. 17 allows three major groups of groundwater to be distinguished. First, G1 groups samples located in the southern areas close to the entrance zone, with points sampled in the separated part of the north indicating that little water evaporative enrichment has taken place (Cenomanian and Triassic aquifer). G2 comprises groundwater located in the broad central part of the plain, implying a mixing of evaporated and

natural water (Quaternary and Pliocene aquifer). Finally, G3 depicts shallow groundwater that is highly evaporated in the borders of low-permeability formations composed primarily of shale and quartzite in the west and by basalts in the east.

The location of surface water in Fig. 17 shows two different behaviors. The strongly evaporated lake waters (p72 and p79) and heavily depleted Mazer Dam waters (p50) are plotted far from groundwater and show no relationship with the groundwater of the study area. However, the location of the waters of the El Haimer dam (p52) and the waters of the ElMalleh River (p56 and p67) are close to that of G3, clearly demonstrating their relationship with the groundwater in this group.

The isotopic enrichment of groundwater by direct evaporation means that the raised salinity observed is, for the most part, a consequence of the concentration of its constituents and predominantly chloride. Moreover, the arrangement of groundwater on the evaporation line and its distribution among the three groups shows a mixing of no less than two end-member waters, natural water, and evaporated water. This result would support the notion that the Berrechid aquifer is essentially recharged by an underflow of sparsely evaporated groundwater originating from the Phosphate Plateau (principally in the intake area), slow surface recharge from rainfall and occasional rivers, and irrigation drainage in the rest of the plain.



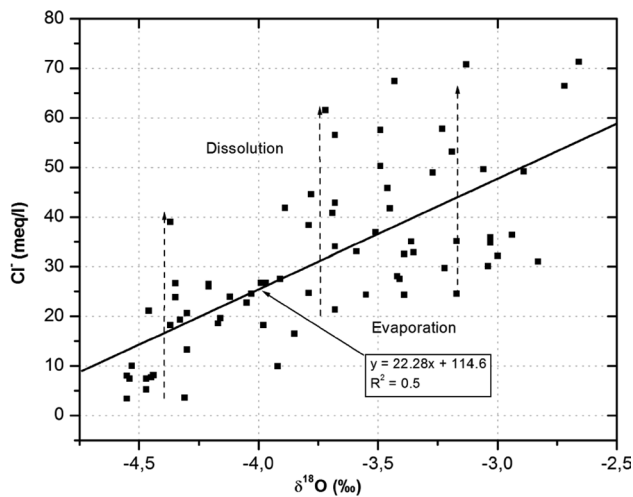


Fig. 18  $\text{Cl}^-$  vs  $\delta^{18}\text{O}$

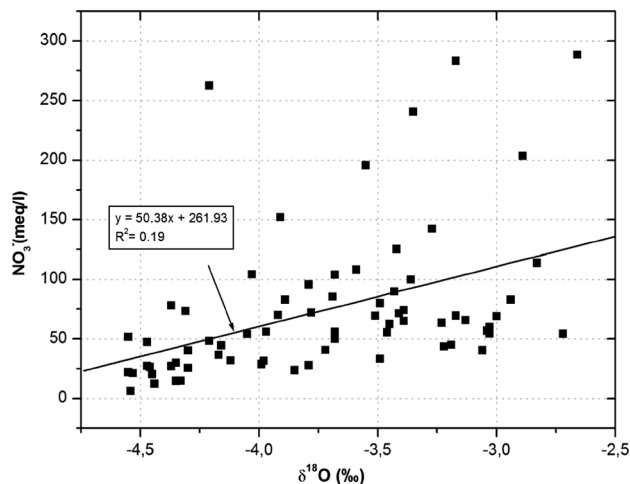


Fig. 19  $\text{NO}_3^-$  vs  $\delta^{18}\text{O}$

### Correlations between isotopic and chemical data

The relationship between conservative elements  $\text{Cl}^-$  and  $\delta^{18}\text{O}$  is further established to demonstrate the importance of the evaporation process and the dissolution of evaporate minerals to the control of groundwater chemical mineralization (Al-Charideh and Abou-Zakhem 2010; Hamed and Dhahri 2013; Boukhari et al. 2015). The data plotted in Fig. 18 shows that chloride concentration correlates well with the oxygen isotope (correlation coefficient = 0.7). This indicates that the evaporative enrichment is reflected in the values of the oxygen isotope, which controls the salinity of groundwater by increasing the concentration of its solutes. On the other hand, some samples' profiles show that chloride concentration increases independently of the

oxygen isotopic composition, inferring the dissolution of salt and evaporate minerals during recharge.

Similarly, Fig. 19 shows that nitrate concentrations increase with the enrichment of oxygen-18 (correlation coefficient = 0.43), demonstrating that the groundwater was meteoric in nature but later changed to its current nature by the concentration of ions due to the evaporation process and anthropogenic activities. These appear to have added significant quantities of nitrate to the groundwater during vertical recharge from rainfall and return irrigation flow. In fact, during successive agricultural cycles, salt accumulates in the soil through evaporation and leaches. Soluble salts move with water and are carried along soil moisture and groundwater flow. Similar features have been observed in investigations conducted in the Souss-Massa Basin, Morocco (Tagma et al. 2009) where an isotopic enrichment in evaporated water and nitrogen-fertilized irrigation water is recharging the aquifer.

Consequently, we conclude that the Berrechid aquifer forms an open hydrological system dominantly recharged by isotopically enriched water. In addition, according to the placement of the points and their isotopic signature, the recharge is achieved by lateral flow of groundwater from the Phosphate Plateau and vertical infiltration from surface water from rainfall, rivers and irrigation return flow.

### Conclusion

The combined hydrochemical and stable isotope ( $\delta^{18}\text{O}$ ,  $\delta^2\text{H}$ ) approach addressed in this study, has provided a better understanding of the functioning of the Berrechid aquifer system and the mineralization processes that underpin the significant compositional variations. Hydrochemical data revealed that the dominating cations and anions are in the order of  $\text{Na}^+ > \text{Mg}^{2+} > \text{Ca}^{2+} > \text{K}^+$  and  $\text{Cl}^- > \text{HCO}_3^- > \text{SO}_4^{2-} > \text{NO}_3^-$ . Regarding TDS and TH classifications, most of groundwater samples are very hard-brackish and only a few are fresh. Three dominant hydrochemical facies are observed in groundwater of the study area: Na–Cl, Na–Mg–Ca–Cl, and Ca–Mg– $\text{HCO}_3$ –Cl. However, a transit toward the Na–Cl of the two ultimate types was noticed. The lowest salinities were observed in the recharge area in the south, with an increasing trend along the flow path, while the highest salinities were located in the eastern and western parts of the plain. The major processes controlling the water quality are the evaporation phenomenon, mixing of saline water with fresh recharge water, cation exchanges, minerals and salt dissolution, and anthropogenic activities. Furthermore, it has been suggested that for brackish waters supersaturated with respect to aragonite, calcite and dolomite, located in the eastern and western parts of the plain, with conditions such high evaporation rate, high ratios of  $\text{Mg}^{2+}/\text{Ca}^{2+}$  and

low concentration of  $\text{SO}_4^{2-}$ , the dolomitization process may occur through a secondary replacement of less soluble minerals (calcite and aragonite) previously precipitated. Shallow groundwater is seriously polluted by nitrates (exceeding 50 mg/l) owing to the anthropogenic activities. Stable isotope data highlighted a significant recharge origin of meteoric water related to an underflow from the Phosphate Plateau along the southern part of the Berrechid basin, as well as by rainfall and irrigation waters infiltration, particularly in areas characterized by poor groundwater quality. In addition, the combination of  $\delta^{18}\text{O}$  values with  $\text{Cl}^-$  and  $\text{NO}_3^-$  concentrations has extended demonstration of the prevalent role of evaporation in increasing salts concentration. Considerable information about the variable nature of groundwater mineralization has been gained through this study, which can help to optimize groundwater resources management and the decision-making process in the Berrechid basin.

**Acknowledgements** The authors are very grateful to the anonymous reviewers for their suggestions and comments which have significantly contributed to the improvement of this manuscript. This work has been achieved with the assistance of the DGH (Direction Générale de l'Hydraulique)/DRPE (Direction de la Recherche et de la Planification de l'Eau)—Rabat—Morocco. The authors gratefully acknowledge the contributions of the ABHBC staff for their help and guidance during the fieldwork. We are also greatly indebted to the technical staff at the laboratories of CNESTEN for their support and sympathy during the laboratory analyzes.

## References

- Abderamane H, Razack M, Vassolo S (2013) Hydrogeochemical and isotopic characterization of the groundwater in the Chari-Baguirmi depression, Republic of Chad. *Environ Earth Sci* 69:2337–2350
- ABHBC (2005) Etude du Plan Directeur d'Aménagement Intégré des ressources en eau du bassin hydraulique du Bouregreg et de la Chaouia. Missions I.2. Évaluation des ressources en eau et des écosystèmes aquatique. Ingema, Scetscom, 2188-192-06b
- Aboulouafa M, Taouil H, Ahmed SI (2016) Assessment of groundwater vulnerability and sensitivity to pollution in Berrechid plain, using drastic model. *Am J Eng Res* 5:10–20
- Ait Brahim Y, Benkaddour A, Agoussine M, Ait Lemkademe A, Al Yacoubi L, Bouchaou L (2015) Origin and salinity of groundwater from interpretation of analysis data in the mining area of Oumjrane, Southeastern Morocco. *Environ Earth Sci* 74:4787–4802
- Ait Sliman A, Fekri A, Laftouhi N, Taj-Eddine K (2009) Utilisation des systèmes d'information géographique et du modèle drastic pour l'évaluation de la vulnérabilité des eaux souterraines dans la plaine de Berrechid, Maroc. *Geogr Techn* 2:81–93
- Al-Charideh A, Abou-Zakhem B (2010) Geochemical and isotopic characterization of groundwater from the Paleogene limestone aquifer of the Upper Jezireh, Syria. *Environ Earth Sci* 59:1065–1078
- Appelo C, Postma D (1993) *Geochemistry, groundwater pollution*, 4th edn. Balkema, Rotterdam
- Bensalah MK et al (2011) The Central Atlantic Magmatic Province (CAMP) volcanic sequences of Berrechid and Doukkala basins (Western Meseta, Morocco): volcanology and geochemistry. *Comun Geol* 98:15–27
- Bouchaou L et al (2009) Origin and residence time of groundwater in the Tadla basin (Morocco) using multiple isotopic and geochemical tools. *J Hydrol* 379:323–338
- Bouchaou L et al (2008) Application of multiple isotopic and geochemical tracers for investigation of recharge, salinization, and residence time of water in the Souss-Massa aquifer, southwest of Morocco. *J Hydrol* 352:267–287
- Boukhari K, Fakir Y, Stigter T, Hajhouji Y, Boulet G (2015) Origin of recharge and salinity and their role on management issues of a large alluvial aquifer system in the semi-arid Haouz plain, Morocco. *Environ Earth Sci* 73:6195–6212
- Bozdağ A (2016) Assessment of the hydrogeochemical characteristics of groundwater in two aquifer systems in Çumra Plain, Central Anatolia. *Environ Earth Sci* 75:1–15
- Clark I, Fritz P (1997) *Environmental isotopes in hydrology*. Lewis Publishers, Boca Raton
- Dansgaard W (1964) Stable isotopes in precipitation. *Tellus* 16:436–468
- Datta PS, Tyagi SK (1996) Major ion chemistry of groundwater in Delhi area: chemical weathering processes and groundwater flow regime. *J Geol Soc India* 47:179–188
- Dindane K, Bouchaou L, Hsissou Y, Krimissa M (2003) Hydrochemical and isotopic characteristics of groundwater in the Souss Upstream Basin, southwestern Morocco. *J Afr Earth Sci* 36:315–327
- Droubi A et al (2008) Development and application of a decision support system (DSS) for water resources management in Zabadani Basin (Syria) and Berrechid Basin (Morocco). Technical Report from the Arab Center for the Studies of Arid Zones and Dry Lands (ACSAD)
- El Assaoui N, Amraoui F, El Mansouri B (2015) Modélisation numérique de l'effet des changements climatiques sur la nappe de Berrechid (Maroc). *Eur Sci J* 11
- El Bouqdaoui K, Aachib M, Blaghen M, Kholtei S (2008) Modélisation de l'écoulement de la nappe de Berrechid (Maroc). *La Houille Blanche* 2:69–75
- El Bouqdaoui K, Aachib M, Blaghen M, Kholtei S (2009) Modélisation de la pollution par les nitrates de la nappe de Berrechid, au Maroc. *Afr Sci Rev Int Sci Technol* 5:99–113
- El Gasmi EH, Mridekh A, El Mansouri B, Tammal M, El Bouhaddoui M (2014) Apport des données géophysiques et géologiques à la mise en évidence de nouveaux éléments structuraux associés à la flexure de Settat (Maroc central). *Bulletin de l'Institut Scientifique*, Rabat
- El Ghali T, Marah H, Qurtobi M, Raibi F, El Mansouri B (2018a) Geochemical evolution of Groundwater in the Quaternary aquifer of the Berrechid Basin, Morocco. *Water Energy Int* 61:54–60
- El Ghali T, Qurtobi M, Marah H, Raibi F, El Mansouri B (2018b) Chemical and isotopic characterization of rainwater in the Berrechid basin. *Moroc J Water Sci Environ Technol* 03:335–341
- El Mansouri B (1993) Structure et modélisation quantitative de l'aquifère de Berrechid Validation par l'approche géostatistique. Université des Sciences et Techniques de Lille, France
- El Mansouri B, Dzikowski M, Delay F, Carlier E, Crampon N (1992) Calage d'un modèle mathématique en régime permanent appliqué à la nappe de Berrechid (Maroc). *Ann Soc Géol Nord* 1:189–193
- Elfarrak H, Hakdaoui M, Fikri A (2014) Development of vulnerability through the DRASTIC method and geographic information system (GIS) (Case Groundwater of Berrchid). *Moroc J Geogr Inf Syst* 6(1):45–58
- Epstein S, Mayeda T (1953) Variation of O18 content of waters from natural sources. *Geochim Cosmochim Acta* 4:213–224

- Fekri A, El Mansouri B, El Hammoumi O, Marrakchi C (2012) Impact of Casablanca municipal landfill on groundwater resources. *Int Water Technol J* 3:210–216
- Fetter CW (1990) Contaminant hydrogeology, 2nd edn. Chemical hydrogeology. Applied hydrogeology. Prentice-Hall/CBS, Upper Saddle River/New Delhi
- Freeze RA, Cherry J (1979) Groundwater. Prentice-Hall, Englewood Cliffs, p 604
- García GM, Hidalgo MdV, Blesa MA (2001) Geochemistry of groundwater in the alluvial plain of Tucuman province, Argentina. *Hydrogeol J* 9:597–610
- Gibbs RJ (1970) Mechanisms controlling world water chemistry. *Science* 170:1088–1090
- Hamed Y, Dhahri F (2013) Hydro-geochemical and isotopic composition of groundwater, with emphasis on sources of salinity, in the aquifer system in Northwestern Tunisia. *J Afr Earth Sci* 83:10–24
- Hanshaw BB, Back W (1979) Major geochemical processes in the evolution of carbonate-aquifer systems. In: *Developments in water science*, vol 12. Elsevier, Amsterdam, pp 287–312
- Hazan R, Moullard L (1962) Notice hydrogéologique de la plaine de Berrechid. Office national des irrigations Services des ressources en eau, Rabat
- HCP (2015) Recensement général de la population et de l'habitat du Maroc 2014. Bulletin officiel No. 6354
- Hem JD (1985) Study and interpretation of the chemical characteristics of natural water, vol 2254. Department of the Interior, US Geological Survey, Reston
- Hoefs J (1997) Stable isotope geochemistry, vol 38, 4th edn. Springer, Berlin, p 41
- Hounslow A (1995) Water quality data: analysis and interpretation. Lewis Publishers, New York
- IAEA (2010) Atlas of isotope hydrology: Morocco. Water Resources Programme, STI/PUB/1480 edn. IAEA, Vienna
- Jankowski J, Acworth RI (1997) Impact of debris-flow deposits on hydrogeochemical processes and the development of dryland salinity in the Yass River Catchment, New South Wales, Australia. *Hydrogeol J* 5:71–88
- Kholtei S, Bouzidi A, Bonini M, Fekhaoui M, Sbai K, Anane R, Creppy EE (2003) Contamination of the water table of the plain of Berrechid in the region of Chaouia, in Morocco, by metals from the wastewaters: influence of rainfall. *Vecteur Environ* 36(5):68
- Kumar M, Ramanathan A, Rao M, Kumar B (2006) Identification and evaluation of hydrogeochemical processes in the groundwater environment of Delhi, India. *Environ Geol* 50:1025–1039
- Lakshmanan E, Kannan R, Kumar MS (2003) Major ion chemistry and identification of hydrogeochemical processes of groundwater in a part of Kancheepuram district, Tamil Nadu, India. *Environ Geosci* 10:157–166
- Liu F, Song X, Yang L, Zhang Y, Han D, Ma Y, Bu H (2014) Identifying the origin and geochemical evolution of groundwater using hydrochemistry and stable isotopes in Subei Lake Basin, Ordos energy base, Northwestern China. *Hydrol Earth Syst Sci Discuss* 11:5709–5745
- Lyazidi A, El Wartiti M, Fadli D (2003) Geodynamic evolution of the Berrechid-ElGara-BenSlimane triassic basin (north-western Meseta, Morocco): depositional dynamics and geometry of sedimentary bodies. *Pangea* 39:23–36
- Machel H-G, Mountjoy EW (1986) Chemistry and environments of dolomitization—a reappraisal. *Earth Sci Rev* 23:175–222
- Machel HG (2004) Concepts and models of dolomitization: a critical reappraisal. *Geol Soc Lond Spec Publ* 235:7–63
- Marah H, Taous F, Qurtobi M, Ouda B, Raibi F (2010) Spatial distribution of Oxygen-18 and Deuterium in precipitation in Morocco. In: EGU General Assembly Conference Abstracts, p 14256
- McLean W, Jankowski J, Lavitt N (2000) Groundwater quality and sustainability in an alluvial aquifer, Australia. In: *Groundwater, past achievements and future challenges*. A Balkema, Rotterdam, pp 567–573
- Ouda O, El Hamdaoui A, Ibn Majah M (2005) Isotopic composition of precipitation at three Moroccan stations influenced by oceanic and Mediterranean air masses. In: *IAEA-TECDOC 2005*, pp 125–140
- Parkhurst DL, Appelo C (1999) User's guide to PHREEQC (Version 2): a computer program for speciation, batch-reaction, one-dimensional transport, and inverse geochemical calculations. *Water-resources investigations report* 99-4259
- Piper A (1953) A graphical procedure in the geochemical interpretation of water analysis, vol 12. USGS Groundwater Note No. 12
- Qurtobi M, Marah H, El Mahboul A, Emblanch C (2010) Groundwater tracing using stable isotope in the western Mediterranean (Case of Rif Chain in the North of Morocco). In: *Advances in research in Karst Media*. Springer, Dordrecht, pp 183–188
- Rajmohan N, Elango L (2004) Identification and evolution of hydrogeochemical processes in the groundwater environment in an area of the Palar and Cheyyar River Basins, Southern India. *Environ Geol* 46:47–61
- Rajmohan N, Elango L (2006) Hydrogeochemistry and its relation to groundwater level fluctuation in the Palar and Cheyyar river basins, southern India. *Hydrol Processes* 20:2415–2427
- Rozanski K, Araguás-Araguás L, Gonfiantini R (1993) Isotopic patterns in modern global precipitation. In: *Climate change in continental isotopic records*. American Geophysical Union, Washington DC, pp 1–36
- Ruhad J (1975) Chaouia et plaine de Berrechid. *Ressources en eau du Maroc, Notes et Mémoires du Service Géologique*, Rabat
- Saadi M, Hilali E, Bensaïd M, Boudda A, Dahmani M (1985) Carte Géologique du Maroc, échelle 1/1000000. Edition du Service Géologique du Maroc. Notes et Mémoires
- Salama R, Farrington P, Bartle G, Watson G (1993) The chemical evolution of groundwater in a first-order catchment and the process of salt accumulation in the soil profile. *J Hydrol* 143:233–258
- Sami K (1992) Recharge mechanisms and geochemical processes in a semi-arid sedimentary basin, Eastern Cape, South Africa. *J Hydrol* 139:27–48
- Sawyer CN, McCarty PL, Parkin GF (2003) *Chemistry for environmental engineering and science*, 5th edn. McGraw-Hill, New York
- Singh AK, Hasnain S (1999) Environmental geochemistry of Damodar River basin, east coast of India. *Environ Geol* 37:124–136
- Smaoui H, Zouhri L, Ouahsine A, Carlier E (2012) Modelling of groundwater flow in heterogeneous porous media by finite element method. *Hydrol Processes* 26:558–569
- Spears D (1986) Mineralogical control of the chemical evolution of groundwater. In: *Trudgill ST (ed) Solute processes*. Wiley, Chichester
- Srinivasamoorthy K, Chidambaram S, Prasanna M, Vasanthavihar M, Peter J, Anandhan P (2008) Identification of major sources controlling groundwater chemistry from a hard rock terrain—a case study from Mettur taluk, Salem district, Tamil Nadu, India. *J Earth Syst Sci* 117:49–58
- Srinivasamoorthy K, Vasanthavigar M, Vijayaraghavan K, Chidambaram S, Anandhan P, Manivannan V (2011) Use of hydrochemistry and stable isotopes as tools for groundwater evolution and contamination investigations. *Geosciences* 1:16–25
- Subba Rao N (2002) Geochemistry of groundwater in parts of Guntur district, Andhra Pradesh, India. *Environ Geol* 41:552–562
- Tagma T, Hsissou Y, Bouchaou L, Bouragba L, Boutaleb S (2009) Groundwater nitrate pollution in Souss-Massa basin (south-west Morocco). *Afr J Environ Sci Technol* 310:301–309
- Van der Weijden CH, Pacheco FA (2003) Hydrochemistry, weathering and weathering rates on Madeira island. *J Hydrol* 283:122–145

- Warner N, Lgourna Z, Bouchaou L, Boutaleb S, Tagma T, Hsaissoune M, Vengosh A (2013) Integration of geochemical and isotopic tracers for elucidating water sources and salinization of shallow aquifers in the sub-Saharan Drâa Basin, Morocco. *Appl Geochem* 34:140–151
- WHO (2004) Guidelines for drinking-water quality: recommendations, 3rd edn, vol 1. WHO, Geneva
- Zaidi FK, Nazzal Y, Jafri MK, Naeem M, Ahmed I (2015) Reverse ion exchange as a major process controlling the groundwater

chemistry in an arid environment: a case study from northwestern Saudi Arabia. *Environ Monit Assess* 187:1–18

**Publisher's Note** Springer Nature remains neutral with regard to jurisdictional claims in published maps and institutional affiliations.